Collaborative Project

CLIM-RUN

Climate Local Information in the Mediterranean region Responding to User Needs

WP2 New Climate modeling and analysis tools
Task 2.1: Analysis of climate information from existing projects

D2.4: Assessment of climate variability and climate change in the Mediterranean region

Project No. 265192– CLIM-RUN

Start date of project: 1st March 2011 Duration: 36 months

Organization name of lead contractor for this deliverable: CMCC

Due Date of Deliverable: September 2013 Actual submission date: October 2013

Authors: A. Bellucci, A. Dell'Aquila, C. Dubois, S. Somot, C. Giannakopoulos

Table of Contents

1. Introduction
2. Sea Level
3. Wind
4. Solar radiation
5. Forest Fire
6. Tourist Climate Index
7. Surface Temperature
8. References

1. Introduction

Climate variability and change in the Mediterranean basin is a subject which, in recent years, has received an increasing amount of interest within the international climate science community. This interest stems from the growing amount of evidence identifying the Mediterranean as a particularly vulnerable region with respect to climate-related changes in (among other aspects) water availability and frequency of extreme weather events (including heat waves, floods and land-slides). Research on Mediterranean climate dynamics has been recently fuelled by a number of initiatives, including both international and European-funded projects. The international initiatives include the MedCLIVAR project (endorsed by the World Climate Research Programme [WCRP]) on climate variability, the MEDEX project (endorsed by the World Meteorological Organization) on high-impact cyclones, the HyMex programme, focusing on the hydrological cycle, and the MedCORDEX framework on regional climate modelling over the Mediterranean domain, contributing to the wider WCRP-sponsored CORDEX program.
Concerning the EU-funded initiatives, an assessment of recently observed modifications of Mediterranean climate and the expected changes for the 21st Century (based on a set climate change scenario simulations performed with high-resolution regional and global coupled general circulation models, under the SRES A1B radiative forcing conditions) was yielded by the FP6 CIRCE project. The provision of information on regional climate change over the wide Euro-Mediterranean sector was also a major outcome of the EU ENSEMBLES project, through a large ensemble of regional climate model (RCM) simulations performed at a 25 Km horizontal resolution (in the atmosphere) for the transient periods 1951-2050 or 1951-2100, under the SRES A1B scenario forcing.
Additional information, but at a typically much coarser horizontal resolution (O(200Km)) is provided by the CMIP3 and CMIP5 multi-model ensembles of long-term simulations, covering pre-industrial, historical and scenario radiative forcing conditions.
Altogether, the experiments performed within CIRCE and ENSEMBLES frameworks represent an impressive set of high-resolution regional scale modelling results, allowing a detailed description of the mechanisms driving climatic variability and change over the Mediterranean region.
Several overview works (including project reports, peer-review articles and books) synthesizing the current understanding on climate variability and change for the Mediterranean region, based on both observational and modelling evidence, have been produced in the recent past. Among the most updated and comprehensive reviews it is worth mentioning the MedCLIVAR project book on "Mediterranean Climate Variability" (Lionello et al. eds., 2006), the IPCC AR4 report (Chapter 11;

Christensen et al. 2007), the CIRCE project report on "Regional Assessment of the Climate Change in the Mediterranean: Air, Sea and Precipitation and Water" (Navarra and Tubiana eds., 2013), and the new MedCLIVAR review book "The climate of the Mediterranean Region: from the past to the future (Lionello ed., 2012; see in particular Chapter 8: The climate of the Mediterranean region in future climate projections, Planton et al., 2012).
In this assessment, the Mediterranean climate variability and change (hereafter MCV) issue is inspected from the peculiar angle of climate products which are relevant to CLIM-RUN. We present an analysis tailored around specific climate variables targeted to user needs, which in turn represent several key sectors of climate services. The report structure reflects this approach, including specific sections on sea-level, wind, solar radiation, forest fires, SST, TCI, each section focusing (where possible) on specific regional case studies.
The analysis is mainly based on the outcomes of ENSEMBLES and CIRCE projects.

2. Sea-level

Sea-level changes have important impacts on the coastal regions, contributing to beach erosion, damages associated with floods and storms, and intrusion of salt in fresh water streams. These impacts, in turn, heavily affect Mediterranean countries, whose coastal economies strongly rely on shore activities.
The sea-level change associated with the steric effect, in particular, has been shown to be substantial (Marcos and Tsimplis, 2008). Combining tide-gauge observations and satellite products, Calafat et al. (2009) suggest that the steric effect in the Mediterranean Sea might produce a trend of sea-level change of 0.3 cm/yr for the 1993-2000 period and 0.1 cm/yr for the 1961-2000 time interval.
Here we inspect the multi-model set of climate projection experiments performed within the framework of the EU CIRCE project to estimate the sea-level change in the Mediterranean Sea due to the steric effect. This analysis is based on the work of Gualdi et al. (2012) and Gualdi et al. (2013), where additional details on the CIRCE models and on the experimental set-up can be found.
Figure 1 shows the evolution of the simulated steric sea level change in the CIRCE integrations from 1951 to 2050, basin-averaged over the Mediterranean Sea. During the reference period (1961-1990), the ensemble-mean tendency is -0.07 ± 0.2 cm/yr. The models produce a rather broad range of trends, varying from the positive values of the ENEA and CNRM models (+0.16 and +0.17 cm/yr, respectively) to the relatively small negative values of the CMCC and MPI simulations (-0.16 and -0.13 cm/yr, respectively) to the large negative value found for the LMD case (-0.57 cm/yr), the latter most likely due to an incomplete spinup of the corresponding model (Gualdi et al., 2013).
Throughout the projected period, all of the CIRCE models show significant positive trends of the steric sea level change (0.29±0.13 cm/yr). The 2021-2050 mean steric sea level rise ranges between +7 and +12 cm, with respect to the reference period. Marcos and Tsimplis (2008), using the A1B CMIP3 simulations, found that the steric effect for the Mediterranean Sea at the end of the twenty-first century might account for an average sea level change ranging between -22 and +18 cm.

In the CIRCE projections, therefore, the range of sea level change appears to be significantly reduced compared to the results of Marcos and Tsimplis (2008). However, the relatively small number of models that form the CIRCE ensemble does not allow a sufficiently robust uncertainty assessment. Thus, based on the present results, it is not possible to attribute the smaller spread to an actual reduction of the uncertainty produced, in turn, by the improved representation of the Mediterranean Sea in the CIRCE models.
Finally, it is worth noting that the CIRCE range of steric change is consistent also with Tsimplis et al. (2008), where at the end of a twenty-first century SRES A2 projection performed with a coupled atmosphere-ocean regional climate model (Somot et al., 2008) the basin-averaged sea level rise is about 13 cm.

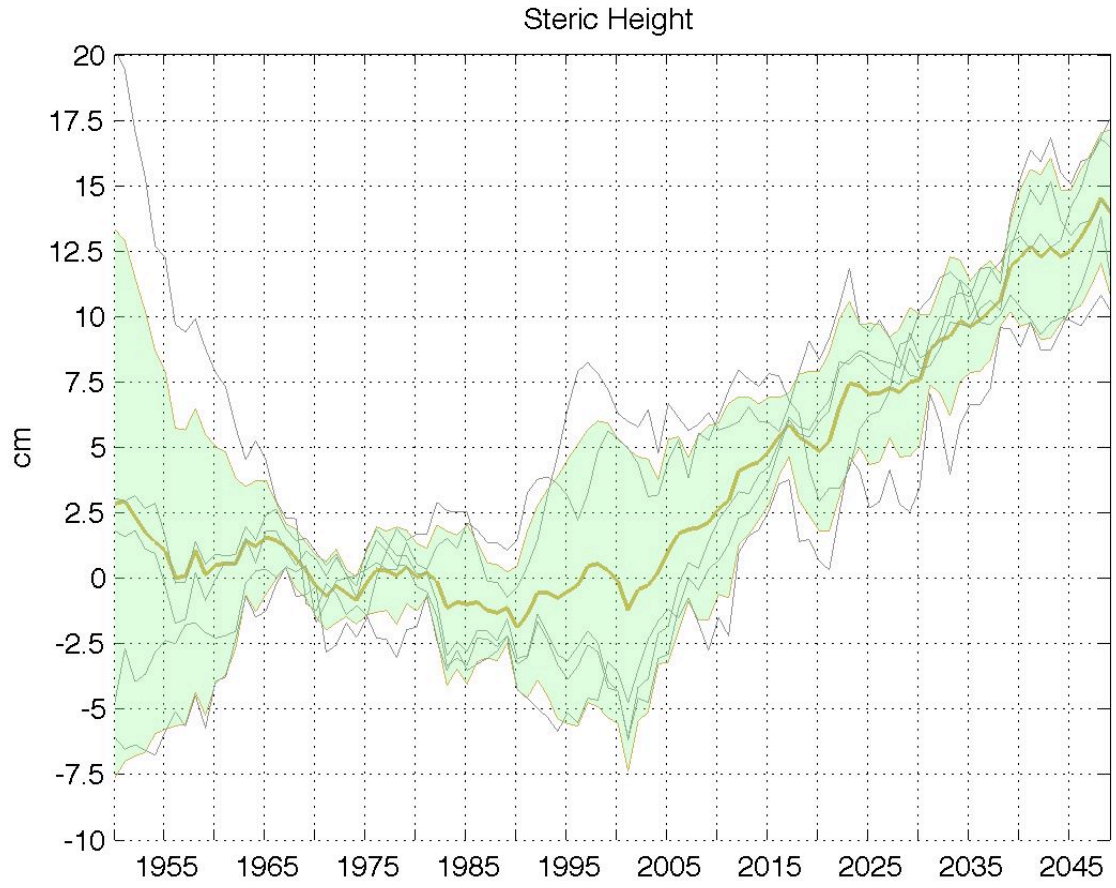

***Fig. 2.1**. Evolution of the steric height anomalies over the Mediterranean Sea from 1951 to 2050 as simulated with the CIRCE models. The anomalies are expressed in cm and have been computed with respect to the 1961–90 mean. Thin lines indicate the individual CIRCE models, the thick curve refers to the CIRCE multimodel mean, and the shading is the CIRCE multimodel standard deviation with respect to the multimodel mean (adapted from Gualdi et al., 2013).*

In a recently published work by Jordà and Gomis (2013; hereafter JG) it is shown that the common practice of using the variability of the steric component to estimate sea-level changes leads to erroneous conclusions on the actual magnitude of regional sea-level rise. In using the total (thermo- plus halo-) steric component, the contribute of salinity to sea-level variability through changes in the total mass of the water body is neglected. In JG it is shown that the mass flux associated with the salinity changes detected in most climate change projections for the Mediterranean Sea significantly affects the sea-level budget for the 21st Century, and therefore needs to be added to the steric effect.

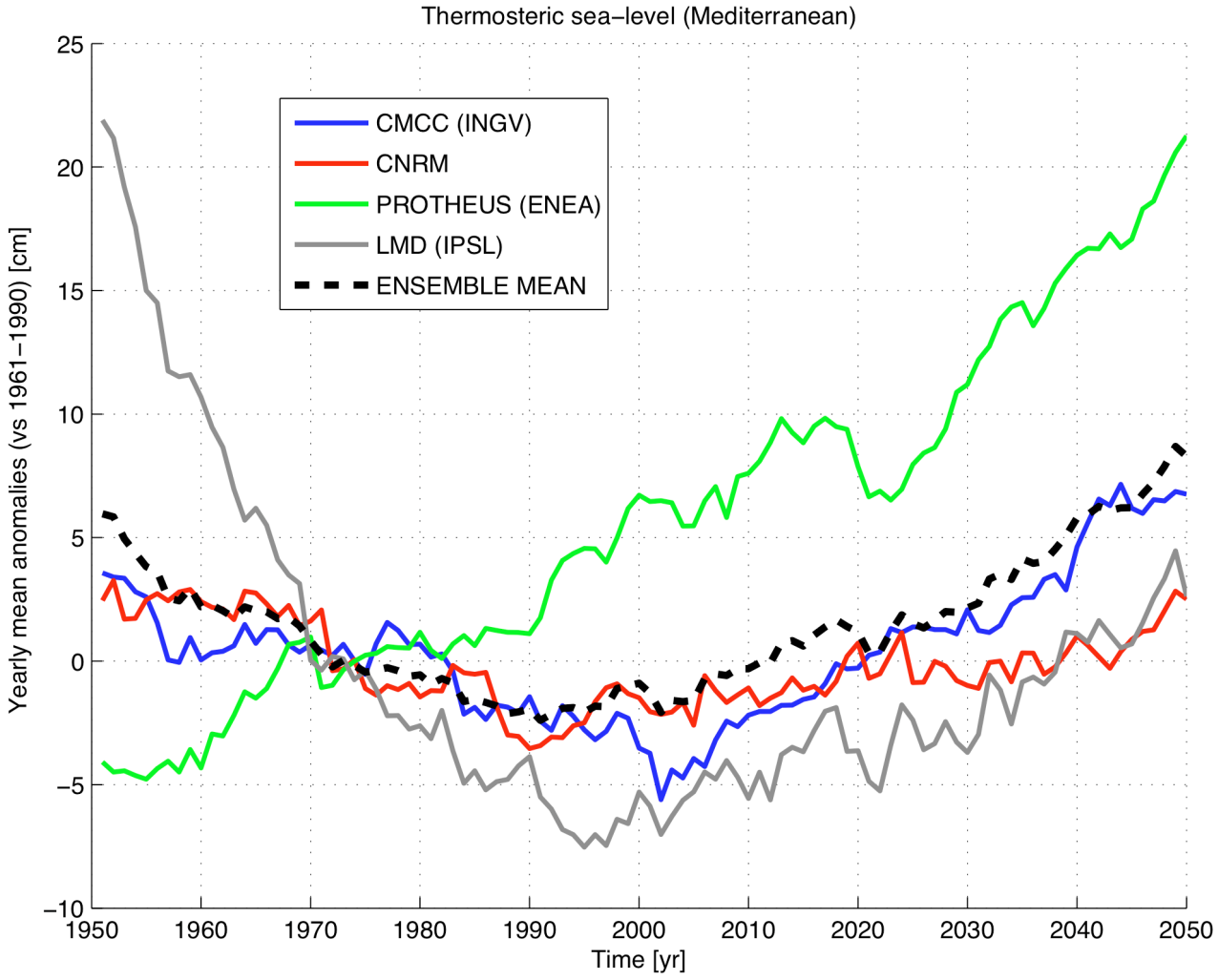

***Fig. 2.2**. Evolution of the thermosteric height anomalies over the Mediterranean Sea from 1951 to 2050 as simulated with four CIRCE models. The anomalies are expressed in cm and have been computed with respect to the 1961–90 mean. The black dashed curve refers to the multimodel mean.*

In particular, the nearly compensating effects of the halo-steric and salt mass change (these two terms being associated with oppositely signed sea-level trends) justify the use of sole thermo-steric effect in quantifying the overall sea-level change (see Fig. 3 in JG).

In light of this result, the CIRCE model-based estimates provided in Gualdi et al. (2013) are revisited, and a sea-level change estimate based only on the thermo-steric component is presented (Fig. 2.2) for the 1951-2050 period (here, only four models from the full CIRCE ensemble are used).
The ensemble mean projected change for the 2001-2050 displays an upward trend of 0.18±0.1 cm/yr amplitude, while the 2021-2050 mean thermo-steric sea level rise (with respect to the reference 1961-1990 period) ranges between -0.7 and +14 cm, around an ensemble average of 4 cm. Thus, with respect to the full steric height estimates provided in Gualdi et al. (2013), a significant reduction for both the trend and the expected changes for the 21st century sea-level is found.
Clearly, steric height-based estimates provide only a partial evaluation of the full sea-level rise signal, as additional components need to be accounted for in a comprehensive estimate of sea-level budget. As reported in the IPCC Fourth Assessment Report (AR4), estimates based on the 1993-2003 well-observed period, show that thermal expansion and melting of land ice (including mountain glaciers, ice caps and Greenland and Antarctica ice sheets) each account for about half of the observed global sea level rise. Land ice is not included in CIRCE models and therefore no GCM-based quantitative estimate is possible with this set of scenario simulations.
To what extent local injections of freshwater determined by the continental ice melting is going to affect the regional patterns of sea level change, and specifically the Mediterranean Sea basin, is highly uncertain, as a number of factors act to shape the local sea level response associated with the meltwater input. Specifically, when ice masses on land melt, the released freshwater is not distributed uniformly over the oceans, due to changes in the Earth's gravity field (Katsman et al., 2008). Also, the local input of fresh and cold water will alter the baroclinic structure of the ocean, and therefore the geostropic circulation (Okumura et al., 2009), which will in turn affect the the sea level topography. Each of these factors is likely to affect the final estimate of sea-level rise in the Meditarranean basin, but an accurate quantification of their final contribution is currently not available.

3. Wind

3.1 Introduction

During the first phase of CLIMRUN, wind fields have been identified as a key climate variable of interest for the case studies on energy (Morocco, Spain) and natural hazards (wild fires, Greece). Most of the interest concerning wind modelling focuses on the very short-range (nowcasting) and on seasonal forecasts, because the largest part of the manageable risk is concentrated on these time-scales. However, the interaction with stakeholders, especially in the energy sector, has highlighted the need for more in depth understanding of wind modelling capacities at a longer time scale, which may contribute to both site evaluation in the absence of very accurate wind atlases and on the assessments of risks that may affect the return on investments on longer time scale.
Recent studies have demonstrated that regional climate models (RCMs) have a large potential for enhancing the quality of climate projections in the presence of complex orography (Artale et al 2010) and in the proximity of coastal areas (Winterfeldt J. and R. Weisse, 2009: Winterfeldt et al.,

2011; Feser et al. 2011). Under CLIMRUN, we have moved one step forward and started the evaluation of wind modelling in the context of today's largest and most consolidated *ensemble* of RCMs produced during the EU-FP6 ENSEMBLES RCMs simulations over Euro-Mediterranean region (Fig.3.1; Christensen et al., 2009).
Purpose of this activity is twofold. First, we wish to address the fundamental issue of uncertainty by highlighting the deficiencies of this particular *ensemble* of climate models in describing specific characteristics of the wind field over the Mediterranean. On the other hand we wish to build examples of the kind of climate information that can be extracted from such a huge - to a large extent still not exploited - resource of model data

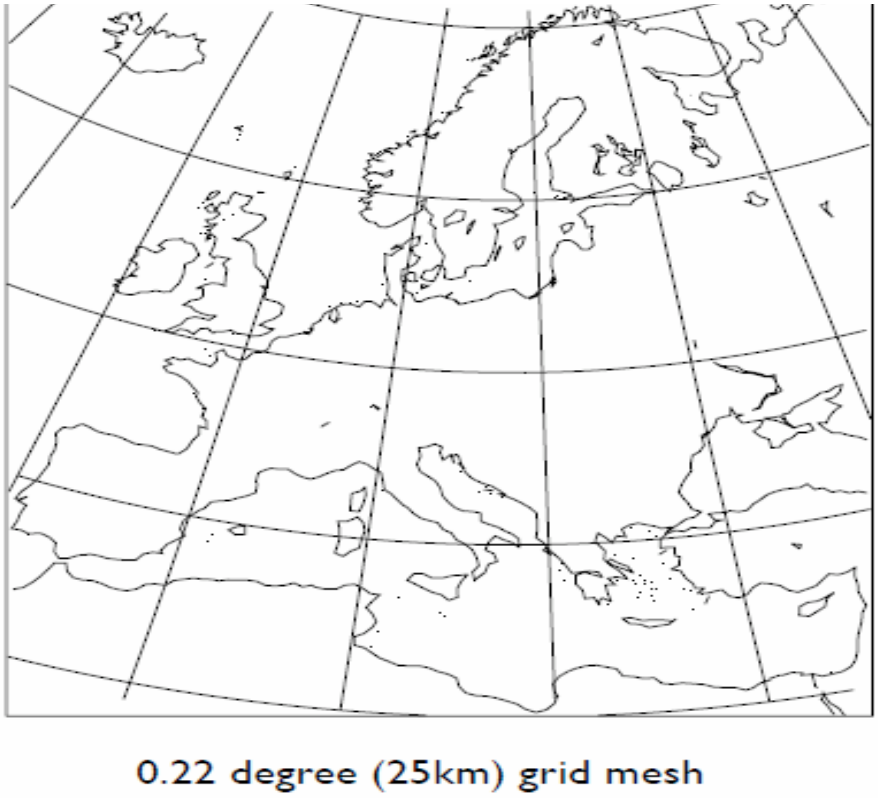

Figure 3.1. *Minimum model domain adopted for the 25km RCM simulation streams over Euro-Mediterranean region during ENSEMBLES. ((http://ensemblesrt3.dmi.dk/)*

3.2 Data

For the assessment of the *ensemble* skill have considered the 10-m wind speed from 12 RCMs control simulations, mostly at a horizontal resolution of 25Km, driven by the global reanalysis ERA40 spanning over the time interval 1961-2000. The evaluation of the model *ensemble* is performed for sea surface wind, for which systematic gridded observation are freely available. The evaluation of wind field over land and has to be left as a subject for a separate study in which the issue of downscaling wind field of wind field over complex topography is addressed carefully.
Here, we compare the model *ensemble* data with the QuikSCAT LEVEL3 observational dataset (Physical Oceanography DAAC, GuideDocument, 2001). This dataset has a global coverage at

daily frequency and a horizontal resolution of 0.5° x 0.5°. The comparison with field observation from moored buoys in a few locations in the Mediterranean shows a mean bias error ranging from -.6 to -.6 m/s and a root mean square error ranging from 1.44 to 2.29 m/s (Ruti et al 2008) .
Note that there is practically no temporal overlap between the control simulations performed during the ENSEMBLES project (1961-2000) and time span of the QuikSCAT data (2000-2009). Therefore we have preliminarily verified the presence of significant trends in the control simulation in order to evaluate the model performances in light of existing long term tendencies. Individual members of the considered *ensemble* present a linear trend over the control period of the order of 0.0001 m/s per year, which is equivalent to a change of about 0.01% per year. On one hand this makes apparently reasonable to compare the two dataset even if they are not overlapping in time. On the other hand, a change in wind field of 0.1% per decade, detected over the control period will have to be compared with the *ensemble* uncertainty and with the tendencies simulated in climate scenarios.
The analysis of the climate scenario is conducted by considering the A1B scenarios produced by using the same RCMs analysed for the control period. In this case the *ensemble* is composed of 16 members, since some of the 12 models evaluated over the control period (HIRAM5,RACMO2,HIRAM) have been driven with multiple global models.
A complete list of the considered regional simulations is reported in Table 3.1.

	Model name	**ERA40 Simulation**	**A1B Scenario**	**A1B Scenario Global driver**
1	C4IRCA3	X	X	HadCM3Q16
2	CNRM-RM4.5	X	X	ARPEGE
3	DMI-HIRHAM5	X	X	ARPEGE
4	DMI-HIRHAM5		X	BCM
5	DMI-HIRHAM5		X	ECHAM5-MPIOM r3
6	ETHZ-CLM	X	X	HadCM3Q0
7	ICTP-RegCM3		X	ECHAM5-MPIOM r3
8	INMRCA3	X		
9	KNMI-RACMO2	X	X	ECHAM5-MPIOM r3
10	KNMI-RACMO2		X	MIROC3.2-hires
11	METNOHIRHAM	X	X	BCM
12	METNOHIRHAM		X	HadCM3Q0
13	METO-HC HadRM3Q16	X		
14	METO-HC HadRM3Q3	X		
15	METO-HC HadRM3Q0	X	X	HadCM3Q0
16	MPI-M-REMO	X	X	ECHAM5-

				MPIOM r3
17	SMHIRCA	X	X	ECHAM5-MPIOM r3
18	SMHIRCA		X	BCM
19	UCLM-PROMES		X	HadCM3Q0

Table 3.1: *Regional climate simulations analysed in this report from ENSEMBLES- RCM data portal (http://ensemblesrt3.dmi.dk/).*

3.3 Validation

In Fig. 3.2 the seasonal *ensemble* average of surface wind speed is presented for the RCMs control simulations during the period 1961-2000. Qualitatively, the *ensemble* provides a realistic description of the main aspects of the wind field over the Mediterranean. Simulated winds are stronger during winter and the maximum intensity is over Gulf of Lion, over the Alboran Sea and over Aegean Sea. Similar features can be also recognized in summer, with a generally weaker wind speed. Instead, a robust pattern of Etesian winds is simulated over the Aegen Sea during summer.

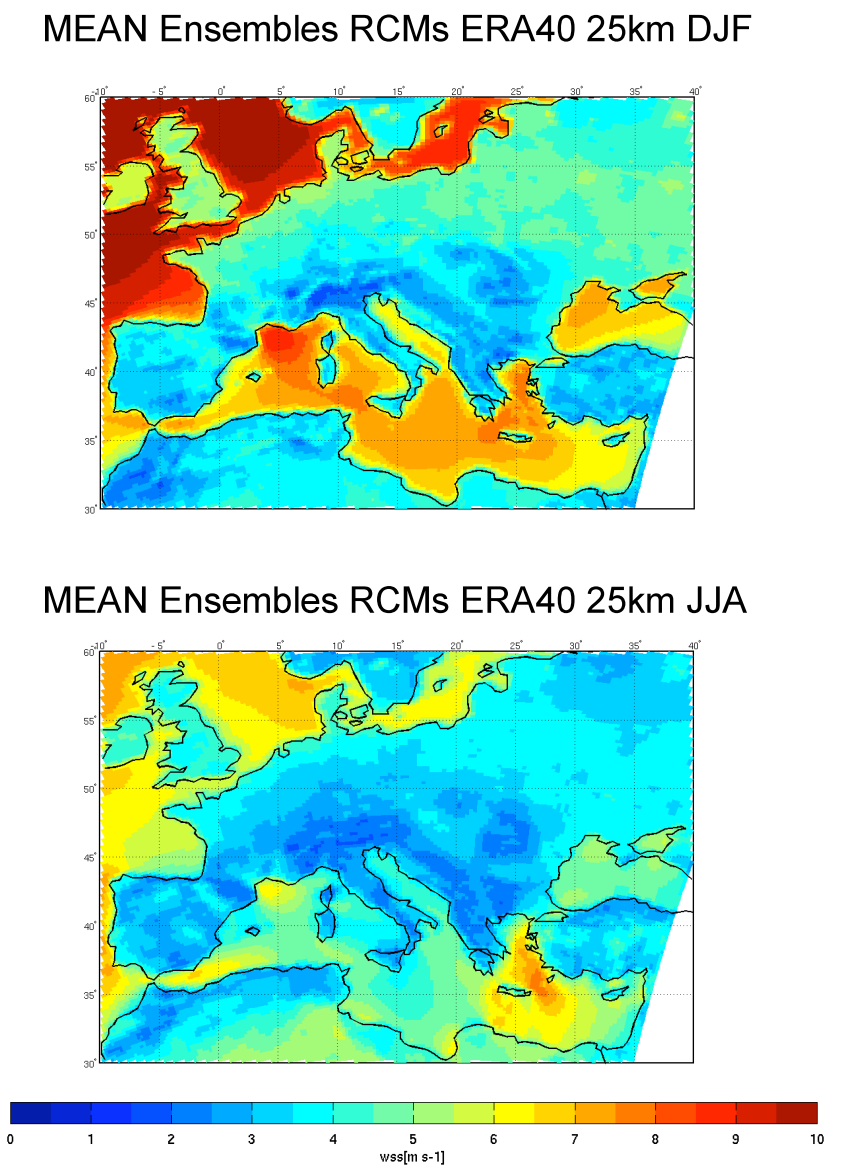

Figure 3.2 *DJF and JJA wind speed ensemble seasonal average for ENSEMBLES RCMs ERA40 simulations.*

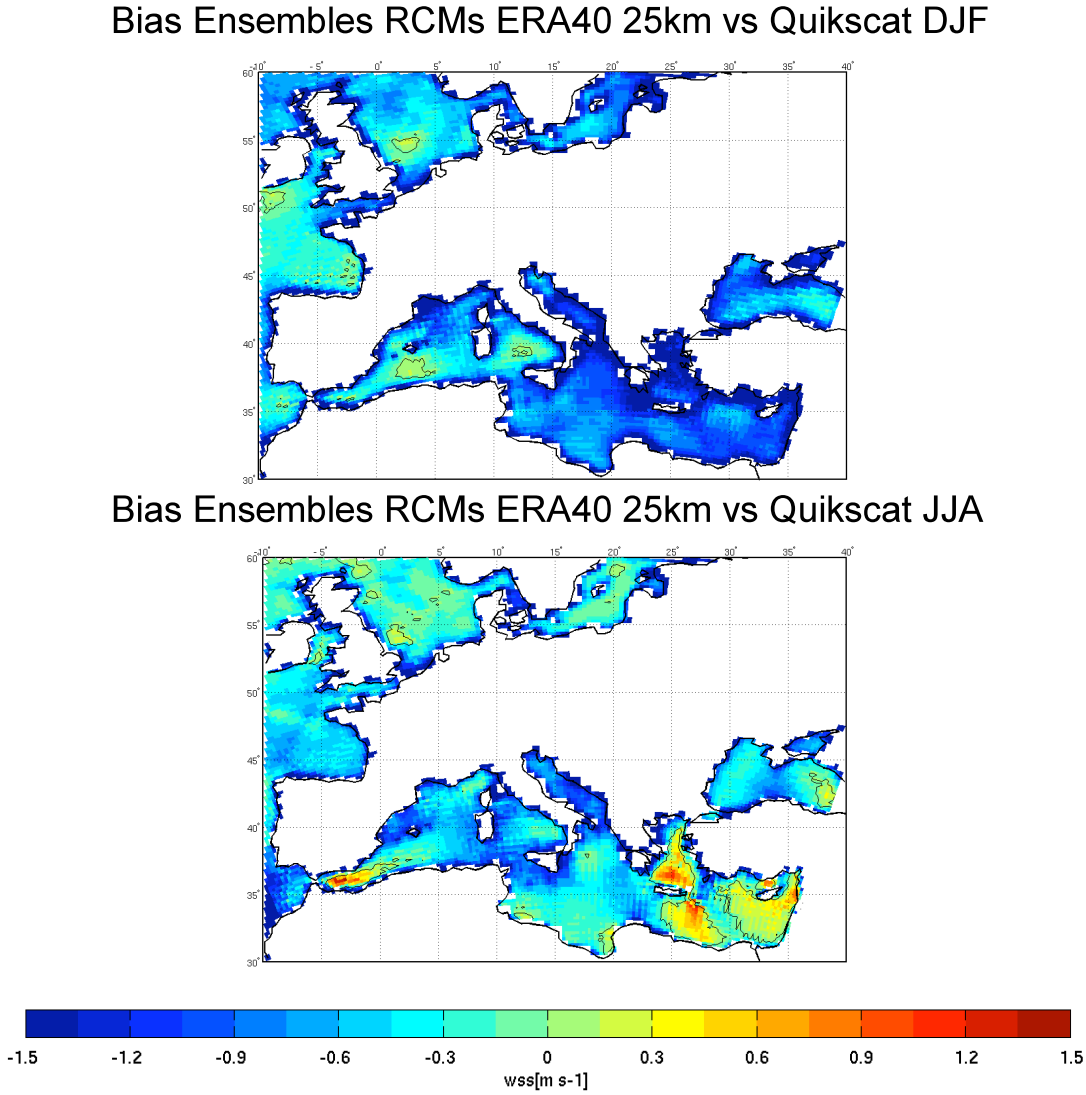

Figure 3.3 *Bias of the ENSEMBLES RCMs ERA40 simulations against QuikSCAT data for the wind speed over sea in winter and summer periods.*

In Fig. 3.3 the mean bias between RCMs simulations and QuikSCAT data is reported for DJF and JJA. In the winter period the ENSEMBLES simulations are affected by a systematic underestimation of wind speed over the whole basin, more accentuated in the eastern basin. On the other hand, during summer an overestimation of Etesian winds can be reported. More in general in the eastern basin an overestimation of the wind field is experienced during summer.

The Root Mean Square Error maps shown in Fig. 3.4 confirm that the greater discrepancies between the wind speed from ENSEMBLES simulations and QuikSCAT observations arise over the Eastern Mediterranean basin during winter.

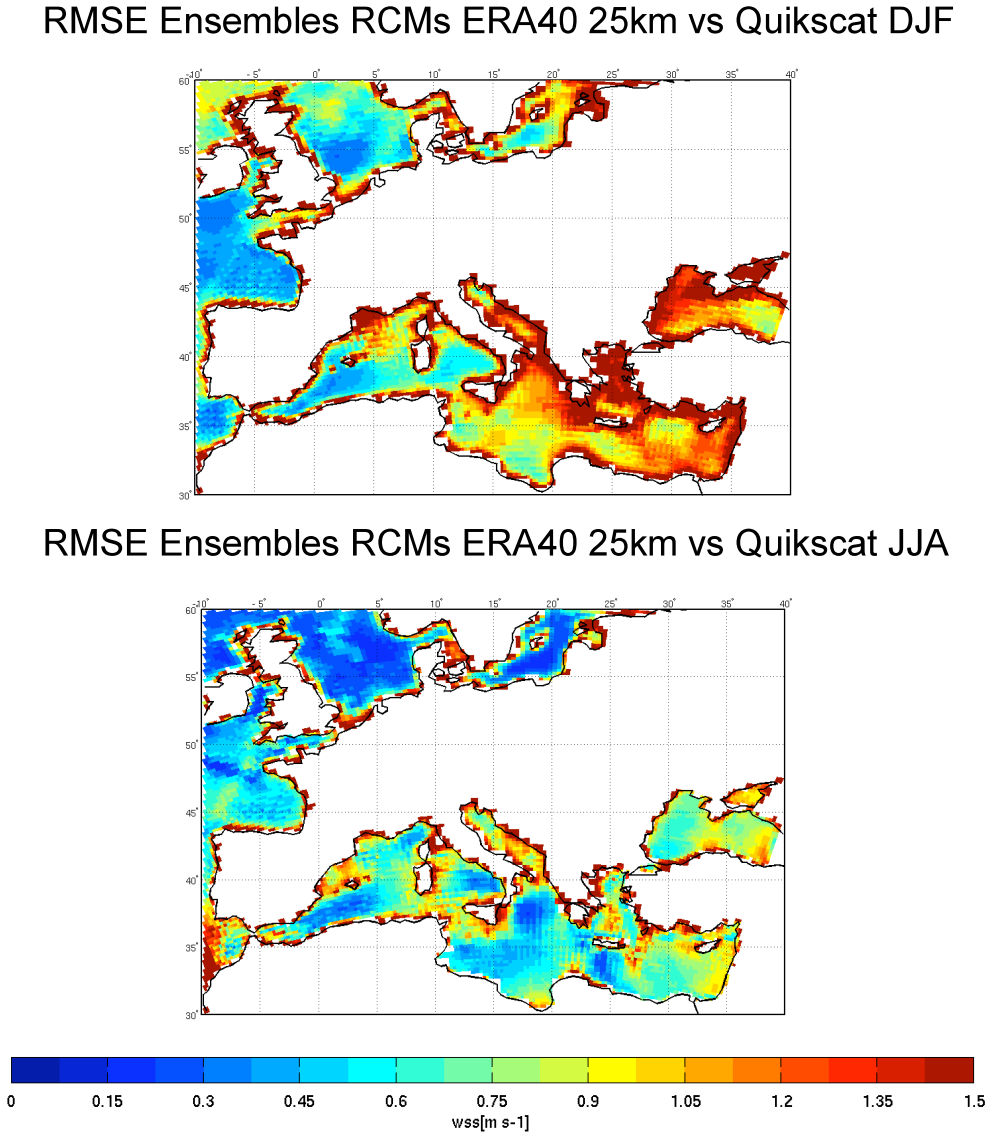

Figure 3.4. *RMSE of the ENSEMBLES RCMs ERA40 simulations against QuikSCAT data for the wind speed over sea in winter and summer periods.*

In Fig. 3.5 we report the *ensemble* spread of the wind speed in the RCMs control simulations, defined as the standard deviation of the seasonal average computed among the *ensemble* members. The cross evaluation of the *ensembles* spread and of the *ensemble* bias, provides useful information concerning the *ensemble* accuracy in the description of the present climate. Therefore, it contributes to a better characterization of the uncertainty to be associated to climate projections especially in view of providing data for downstream impact studies. If a substantial *ensemble* bias is detected in a region of limited spread, it is possible to effectively remove the *ensemble* bias by subtracting it from each member of the *ensemble* and even relatively small changes produced in climate scenarios may be detected. On the other hand, in case of a small *ensemble* bias and a large *ensemble* spread,

changes in the wind regimes can be detected only when they become sufficiently large. Obviously, in the case of large bias and large spread it is difficult to both correct the *ensemble* average and to detect potential changes.

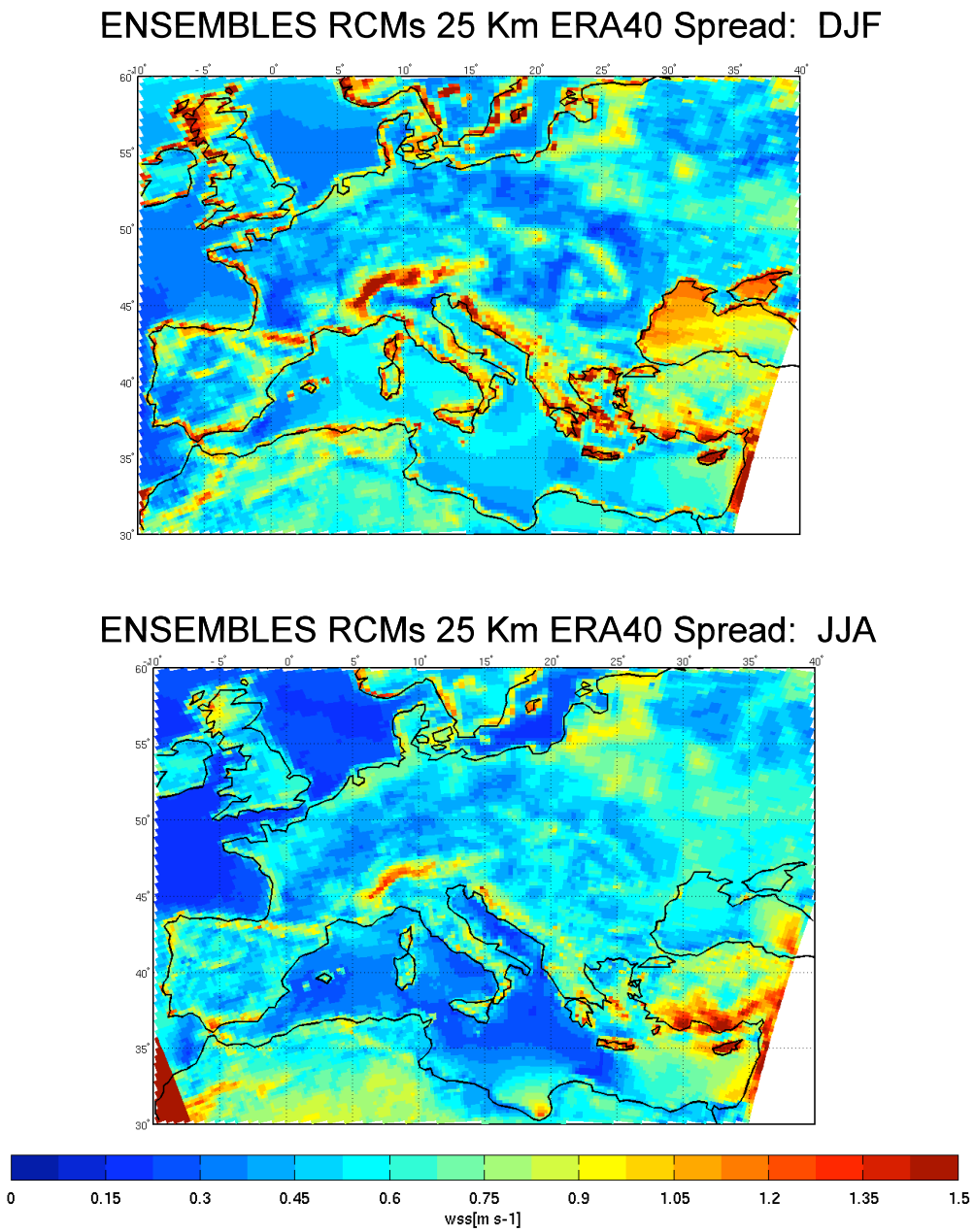

Figure 3.5. *Spread of the ENSEMBLES ERA40 RCMs simulations for the wind speed seasonal average for (top) DJF and (bottom) JJA.*

The higher *ensembles* spread is found along the coasts in the proximity of complex orography (Alps, Balkans, Pyrenees, Greece) where the wind speed can be highly affected by the

representation of orography and land sea mask of the single models and by the representation of air-surface interaction processes.
Over Atlantic the *ensemble* spread is generally quite low because the wind field in this area is strongly constrained to the boundary conditions, and there is no topographic feature affecting the large scale pattern. Over Mediterranean sea the largest *ensemble* spread can be found in the Levantine Basin and Aegean sea, especially during summer in the region of Etesian winds. These discrepancies can be attributed to the complex orography of Aegean region that can be modify surface wind fields. The regional models need an higher horizontal resolution to correctly reproduce those small scale features. During winter a large *ensemble* spread can be detected in the western Mediterranean basin, while in the Levantine the spread exhibits an increase during summer.

3.4 Scenario

After the validation step above described, we have analysed the SRES A1B RCMs ENSEMBLES simulations reported in table1 in terms of future changes of monthly wind speed.
The maps reported in Fig. 3.6 show the projected changes in 10m wind speed over the Mediterranean. The map is obtained by averaging the winter and summer mean wind speed changes foreseen in ENSEMBLES RCMs scenario for 2021-2050 against 1961-1990. Hatched areas represent areas where more than 66% of simulations agree in the sign of the long term change. According to those projections, most of the Mediterranean region is expected to see a decrease in mean wind speed during winter especially in the southern part of the basin.
It is useful to discuss figure 6 by considering the relative importance of the *ensemble* bias and of the *ensemble* spread in characterizing the uncertainty of climate projections (section 3.3).
During summer the tendency over the Western Mediterranean and over the Ionian sea is relatively weak. However, given the correspondingly small *ensemble* spread (figure 3.5), a majority of the members of the *ensemble* agree at least in the sign of the tendency. On the other hand, during winter a larger *ensemble* spread is detected over most of the basin (figure 3.5). However the long term tendency is also relatively large and a weakening of the wind field is a common characteristic of the majority of the *ensemble* members.
The Levantine and the Aegean sea are characterized by both a large bias and a relatively large *ensemble* spread thereby indicating a common difficulty in the modelling of wind regimes in this particular area of the Mediterranean.

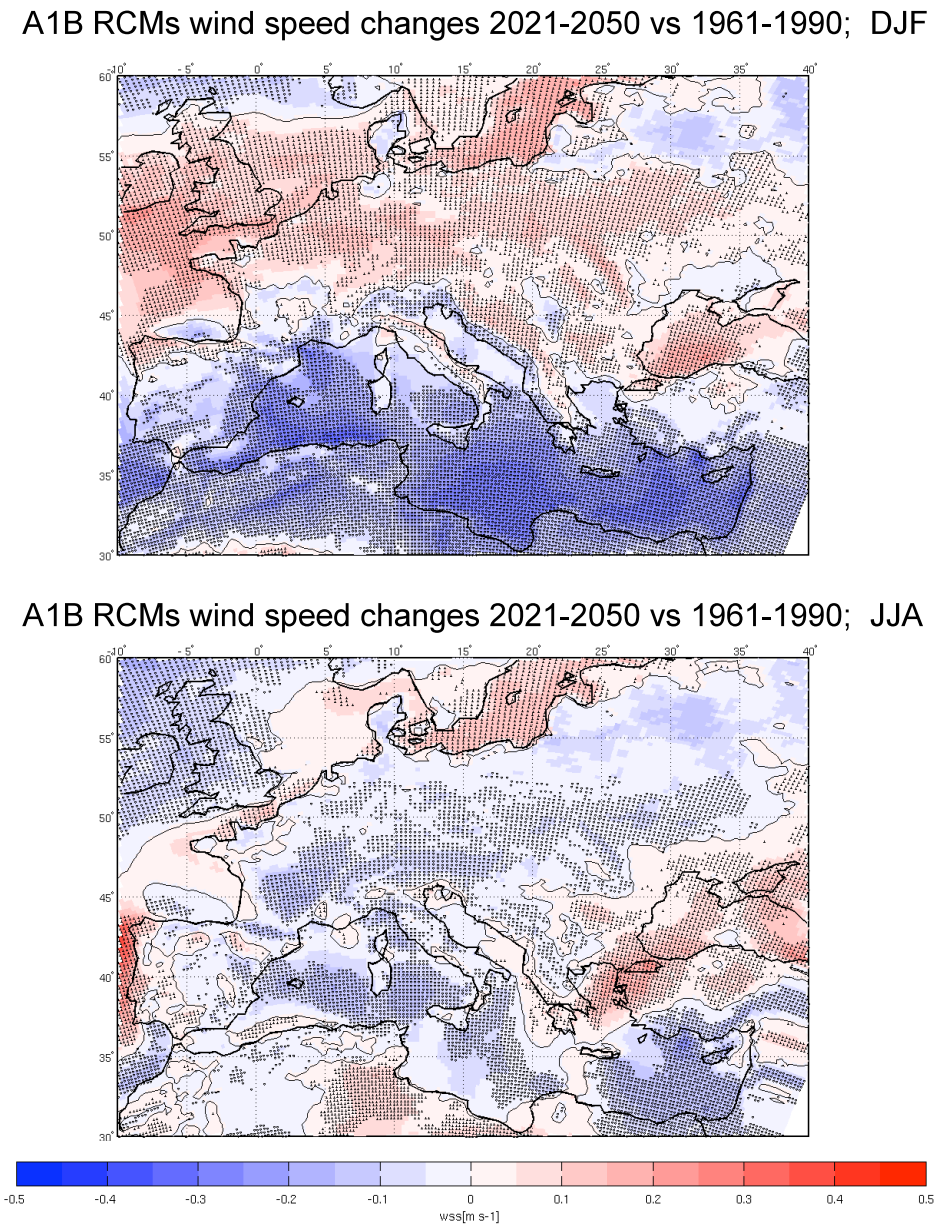

Figure 3.6: *Mean change in surface wind speed projected by A1B scenario RCMs ENSEMBLES simulations. Colours represent the average long term change in wind speed projected for 2021-2050 with respect to 1961-1990. Model data are produced at an horizontal resolution of about 25Km with the exception of KNMI-RACMO2 simulation driven by MIROC that has been produced at 50km . Hatched areas represent areas where more than 66% of the model agree in the sign of the long term change.*

In order to better highlight the projected climate changes in wind speed from ENSEMBLES simulations over the regions of interest for CLIMRUN case studies, we have finally produced histogram plots for wind speed changes averaged over two boxes over Greece (Forest Fires CLIMRUN case study) and over Morocco (Energy CLIMRUN case study).

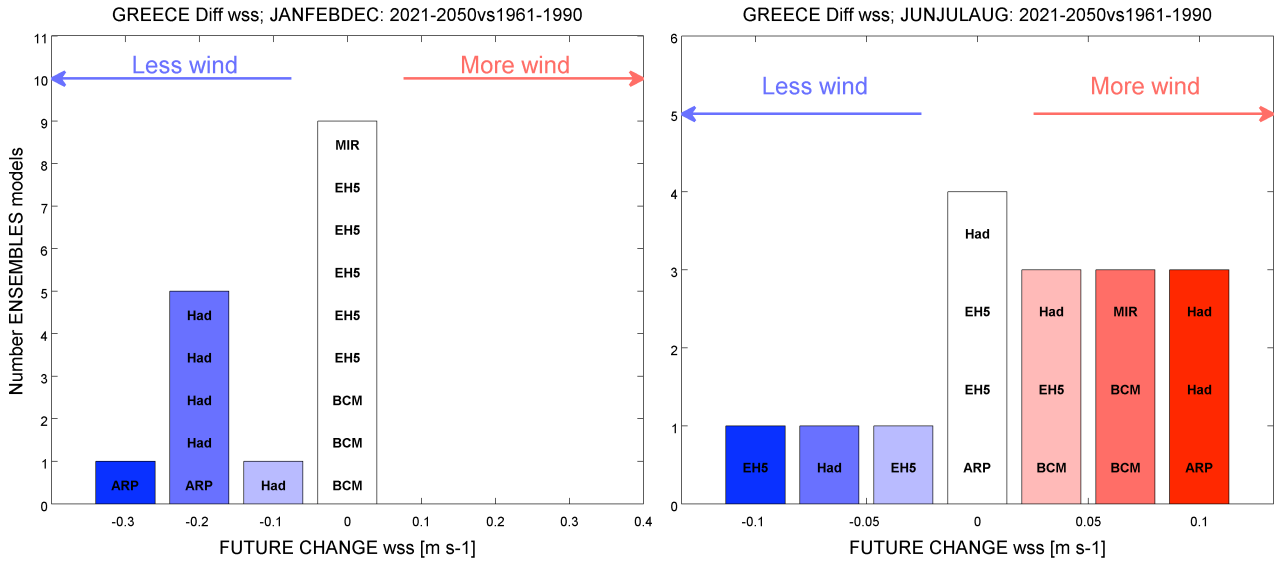

Figure 3.7 *Histogram of SRES A1B RCMs ENSEMBLES simulations (with the corresponding global drivers) for foreseen changes in wind speed over a box (LON: 19-25E; LAT=36-41N) enclosing Greece. We report the projected changes for the 2021-2050 period against 1961-1990.*

In Fig. 3.7 we report the future changes for the 2021-2050 period against 1961-1990 in wind speed over Greece as projected by ENSEMBLES RCMS simulations. During winter the most part (9 /16) of simulations show no relevant changes in wind speed while the others features a general decrease of wind speed. During summer the major part of the simulations (9/16) exhibits an increase of wind speed. Only three simulations project a decrease of summer wind speed in Greece. This information can be potentially relevant to identify new possible regions vulnerable to wildfires risk and in the management of existing and new forests.

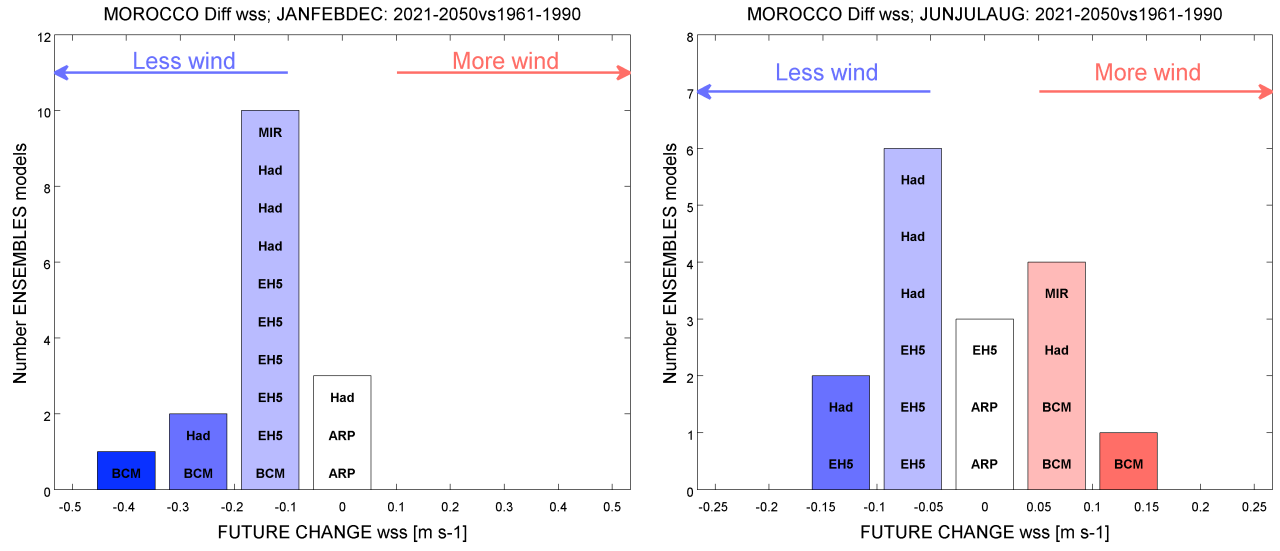

Figure 3.8 *Histogram of SRES A1B RCMs ENSEMBLES simulations (with the corresponding global drivers) for foreseen changes in wind speed over a box (LON:7W-1E; LAT=32-36N) enclosing Morocco. We report the projected changes for the 2021-2050 period against 1961-1990.*

Similarly, in Fig. 3.8 we report the future changes for the 2021-2050 period against 1961-1990 in wind speed over Morocco as projected by ENSEMBLES RCMS simulations. During winter the most part (13 /16) of simulations show a decrease in wind speed. During summer the projections are more scattered even if in 8 simulations a decrease of wind speed is obtained. According to those projections, the here considered region (and more in general the Southern part of Med basin, see Fig 3.6) is expected to see a decrease in mean wind speed which would imply an overall loss of the expected productivity in wind energy sector.

4. Solar radiation

4.1 Introduction

For the case study on energy, the downward solar radiation has been identified as a key climate variable of interest over Morocco and Spain. Interaction with stakeholders has highlighted the need for more information of solar radiation on longer time scales which can be useful to assess the return on investments in the long term. Here, we use scenario simulations performed with an ensemble of regional climate models (RCM) in the framework of the ENSEMBLES Project, to assess future changes in solar radiation over the Mediterranean region.

4.2 Data

For the assessment of the ensemble skill we have considered the surface solar downward radiation (rsds) from 12 RCMs simulations, mostly at a horizontal resolution of 25 km, driven by the global reanalysis ERA40 spanning over the time interval 1984-2000, overlapping with NASA GEWEX Solar Observation gridded dataset.
The analysis of the climate scenario is conducted by considering the A1B scenarios produced by using the same RCMs analysed for the control period. In this case the ensemble is composed of 16 members, since some of the 12 models evaluated over the control period (HIRAM5,RACMO2,HIRAM) have been driven with multiple global models.
A complete list of the considered regional simulations is reported in Table 4.1.

	Model name	ERA40 Simulation	A1B Scenario	A1B Scenario Global driver
1	C4IRCA3	X	X	HadCM3Q16
2	CNRM-RM4.5	X	X	ARPEGE
3	DMI-HIRHAM5	X	X	ARPEGE
4	DMI-HIRHAM5		X	BCM
5	DMI-HIRHAM5		X	ECHAM5-MPIOM r3
6	ETHZ-CLM	X	X	HadCM3Q0
7	ICTP-RegCM3		X	ECHAM5-MPIOM r3
8	INMRCA3	X		
9	KNMI-RACMO2	X	X	ECHAM5-MPIOM r3
10	KNMI-RACMO2		X	MIROC3.2-hires
11	METNOHIRHAM	X	X	BCM
12	METNOHIRHAM		X	HadCM3Q0
13	METO-HC HadRM3Q16	X		
14	METO-HC HadRM3Q3	X		
15	METO-HC HadRM3Q0	X	X	HadCM3Q0
16	MPI-M-REMO	X	X	ECHAM5-MPIOM r3
17	SMHIRCA	X	X	ECHAM5-MPIOM r3
18	SMHIRCA		X	BCM
19	UCLM-PROMES		X	HadCM3Q0

Table 4.1: *Regional climate simulations analysed in this report from ENSEMBLES- RCM data portal (http://ensemblesrt3.dmi.dk/).*

In our study we used rsds data from the NASA/GEWEX SRB project which has as the objective to determine surface, top-of-atmosphere (TOA), and atmospheric shortwave (SW) and longwave (LW) radiative fluxes with the precision needed to predict transient climate variations and decadal-to-centennial climate trends. The data includes the time interval starting no later than July 1983 and currently extending to December 2007. The horizontal resolution of the global grid is 1° x 1°. References about the algorithm can be found in the following papers: Pinker and Laszlo 1992, Fu et al.1992, Gupta et al. 2001 and Gupta et al.1992. The algorithm was largely validated with data obtained by Baseline Surface Radiation Network (BSRN), the Swiss Federal Institute of Technology's Global Energy Balance Archive (GEBA) and NOAA's Climate Monitoring and Diagnostics Laboratory (CMDL). Results of daily monthly averaged SW radiative fluxes show that generally flux errors are within 35.7 Wm-2. Larger errors were found where there are larger

uncertainties in the input data such as over snow/ice covered surfaces and where the site data did not represent the entire grid box. Larger errors in downward SW flux were also found over African and South American locations where aerosols from biomass burning are not accounted for in the SW model (Konzelman et al., 1996). Moreover it must be considered that SRB algorithms rely heavily on radiances and cloud properties from ISCCP and there are a few known issues and discontinuities in the ISCCP products which are likely to be reflected in SRB products, all of them are listed in the GEWEX websites.

4.3 Validation: RCMs ENSEMBLES ERA40 simulations

In Fig. 4.1 the mean bias between RCMs simulations and NASA Solar data is reported for DJF and JJA. In the winter period the ENSEMBLES simulations are affected by a systematic underestimation of rsds over the most part of the Euro-Mediterranean region, more accentuated over the sea. Positive anomalies are present over North Africa and more in general over the coastal eastern Mediterranean regions, probably due to an inadequate description of cloud cover over arid and semi-arid soils in the regional models. For summer period the models experience a strong systematic underestimation of rsds over sea and a general overestimation over the south-central Europe, especially in the eastern part of the continent and over Anatolian peninsula. The RMSE maps (Fig. 4.2) confirms these features with a winter relative maximum over the sea and with overall high values over the sea (likely related with the convection parameterizations adopted in the models) and over the central-eastern Europe. This feature can be ascribed to strong changes in the aerosols distribution over eastern Europe occurred in the last part of XX century and not included in the models that mainly report only climatological values for aerosols distribution.
In Fig. 4.3 we report the *ensemble* spread of rsds in the RCMs evaluation simulations, defined as the standard deviation of the seasonal average computed among the *ensemble* members and the standard deviation divided by the seasonal mean, respectively. The cross evaluation of the *ensembles* spread and of the *ensemble* bias/RMSE against observations provides useful information concerning the *ensemble* accuracy in the description of the present climate. Therefore, it contributes to a better characterization of the uncertainty to be associated to climate projections especially in view of providing data for downstream impact studies. If a substantial *ensemble* bias is detected in a region of limited spread, it is possible to effectively remove the *ensemble* bias by subtracting it from each member of the *ensemble* and even relatively small changes produced in climate scenarios may be detected. On the other hand, in case of a small ensemble bias and a large *ensemble* spread, changes in the solar downward radiation can be detected only when they become sufficiently large. Obviously, in the case of large bias and large spread it is difficult to both correct the ensemble average and to detect potential changes.
The winter spread (generally characterised by lower values as the smaller seasonal mean solar radiation present in winter) shows its maximum over the Southern Mediterranean. This feature is present also in summer when higher values are present over sea and over the mountains, probably linker with different representation of topography and of the corresponding topographic uplift in the RCMS simulations.

4.4 Scenario: RCMs ENSEMBLES SRESA1B simulations

Future changes in the total downwelling shortwave radiation reported in Fig. 4.4 shows a well defined regional pattern. We compare the average seasonal radiation for the periods 2012-2050 and 1961-1990. At the large scale, the regional pattern of change in incident solar radiation is quite robust throughout the year: solar radiation decreases in northern Europe, roughly above 45° north, whereas it increases in the Euro-Mediterranean area, south of the same latitude.
By considering the differences of solar radiation that are significant at the 90% confidence level according to a t-Student test on the corresponding distributions of their monthly values, most of the ensemble members agree in the sign of the projected changes.
The regional patterns of the projected changes however differ significantly depending on the season. We consider the winter (DJF) and summer (JJA) season to illustrate the most important differences that originate inside the considered domain. During winter, the largest decrease in downwelling radiation is produced to the north-east of the considered domain, whereas during summer the area of significant decreasing trend is shifted towards the north west part of the domain. The seasonality of the changing pattern is associated to large scale atmospheric circulation features. In fact, a similar pattern of seasonal change is also present in the corresponding global drivers (Fig. 4.5) and in the corresponding patterns of cloud cover changes (not shown here).
In the southern part of the considered domain, significant differences between the winter and summer changes can be detected. During winter a zonal band of increasing solar radiation is centered over the Mediterranean Sea, with areas of particularly large increase (above 4 W/m^2) over north Africa and over the Levantine basin. Instead, during summer the area over north Africa is already mostly cloud free and no significant changes are produced in the scenarios. Instead, the areas that are subject to substantial decrease in cloudiness and rainfall during summer (the north western Iberian Peninsula, the area of the Balkans and the Anatolia) correspond also to the areas where the largest increase in incident solar radiation is produced.
Boé et al. (2009) have suggested that for the ENSEMBLES models over northern Europe the driving GCM's are the main source of model uncertainty. Instead the role played by the global driver over southern Europe on multi-model mean precipitation changes is generally weak. In particular Déqué et al. (2012) have pointed out that for the A1B emissions scenario and 2021–2050 time slice, a large role is played the RCMs in characterizing the uncertainty of summer precipitation.
Consistently, we find out that during winter the regional models follow rather closely the global drivers, both in the north and in the south of the domain. Instead, during summer the regional models produce a rather different pattern of changes than the corresponding ensemble of global drivers (Fig. 4.5). In fact the strong meridional differences in the regional scenarios discussed above correspond, in the global drivers, to a more uniform signal of increasing incident radiation.

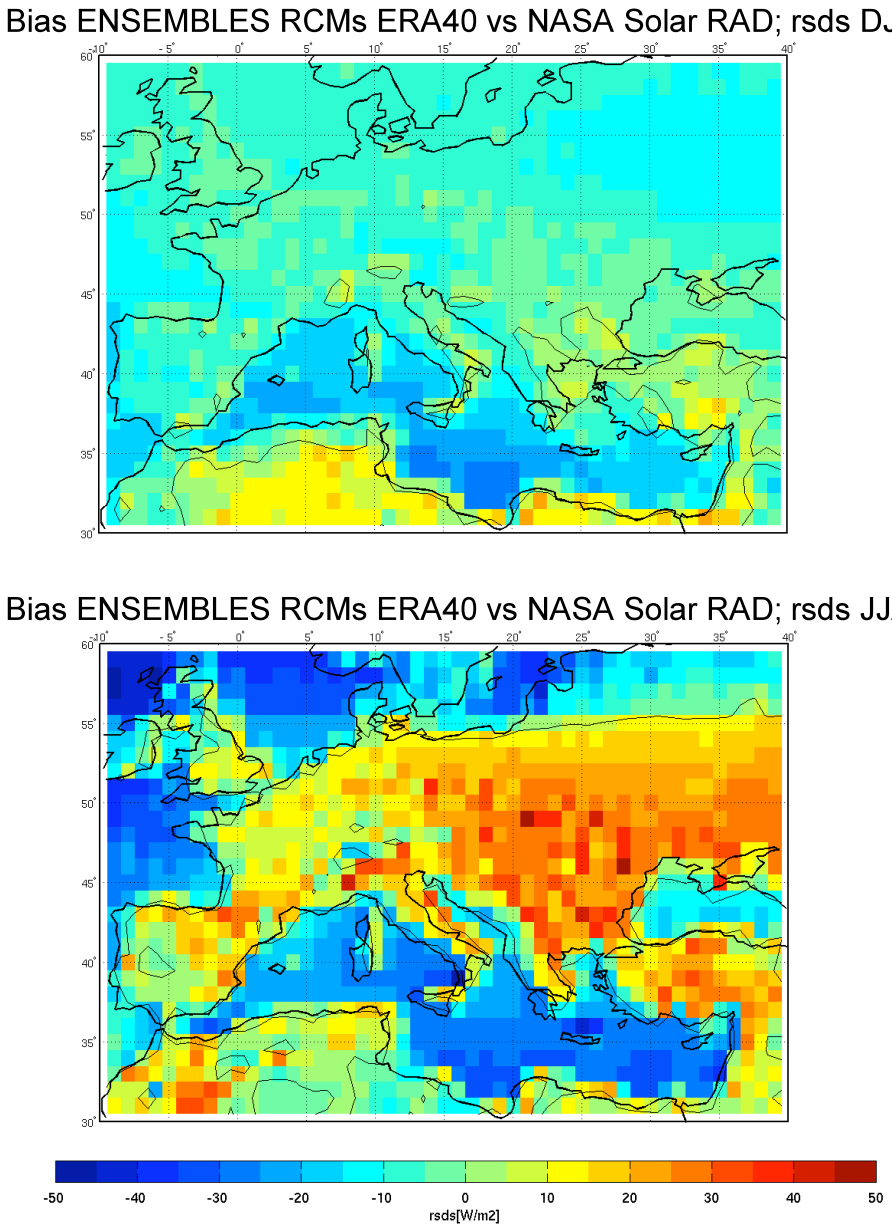

Figure 4.1 *Bias of the ENSEMBLES RCMs ERA40 simulations against NASA Solar Radiation data for rsds in winter and summer periods.*

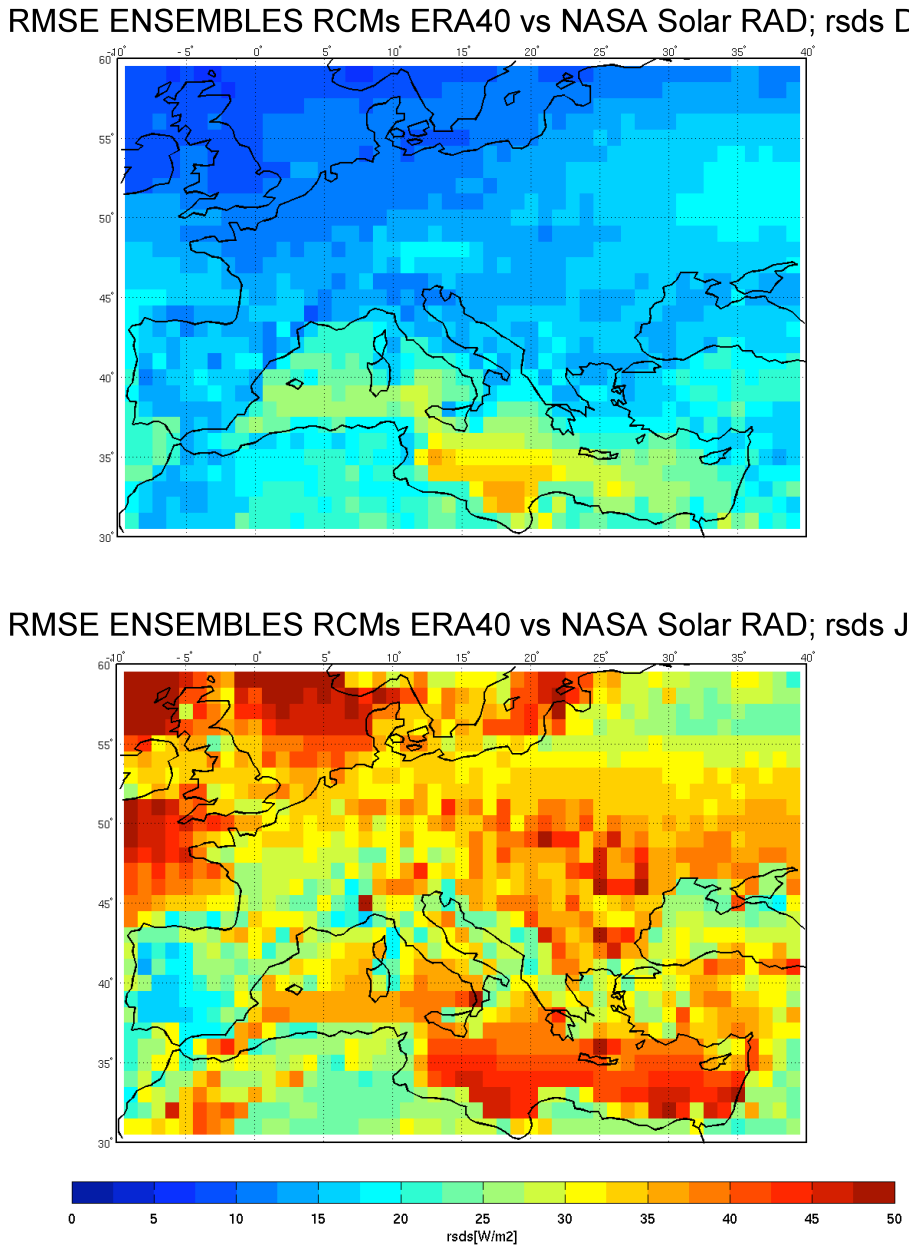

Figure 4.2 *RMSE of the ENSEMBLES RCMs ERA40 simulations against NASa solar radiation data in winter and summer periods.*

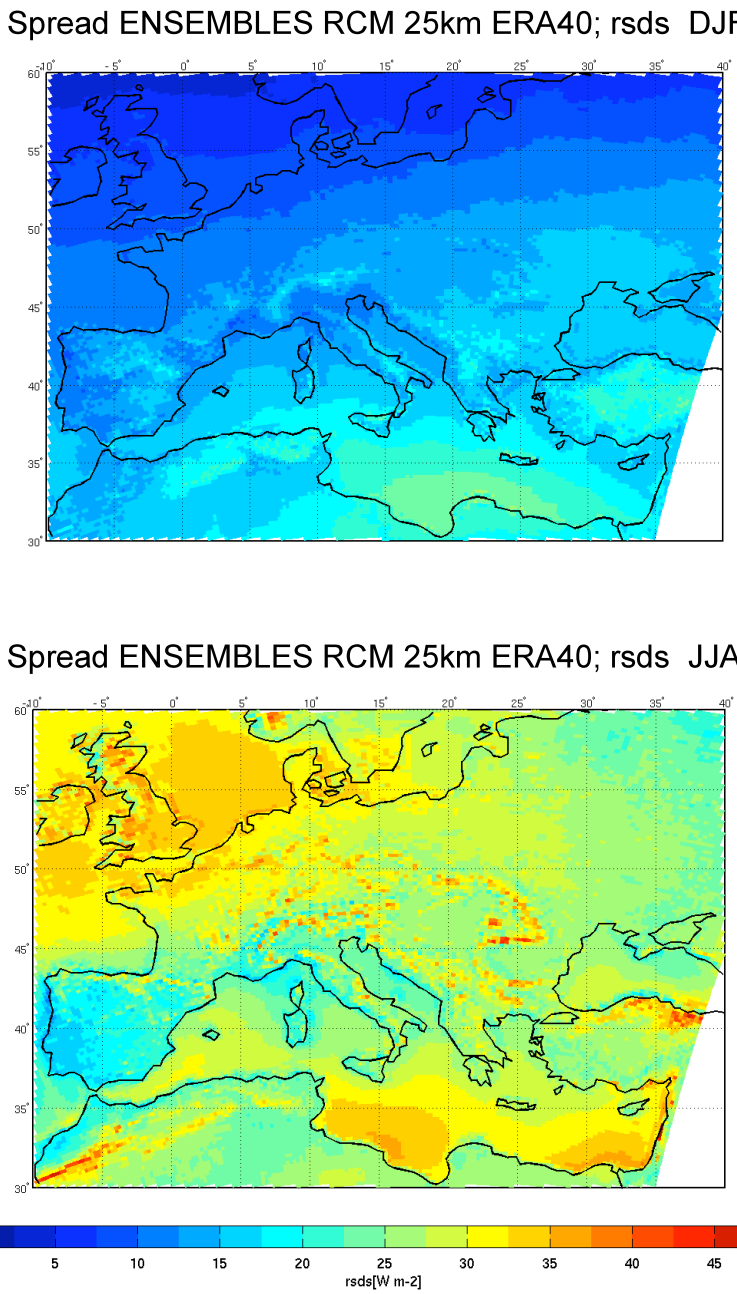

Figure 4.3 *Spread of the ENSEMBLES ERA40 RCMs simulations for the rsds seasonal average for DJF and JJA*

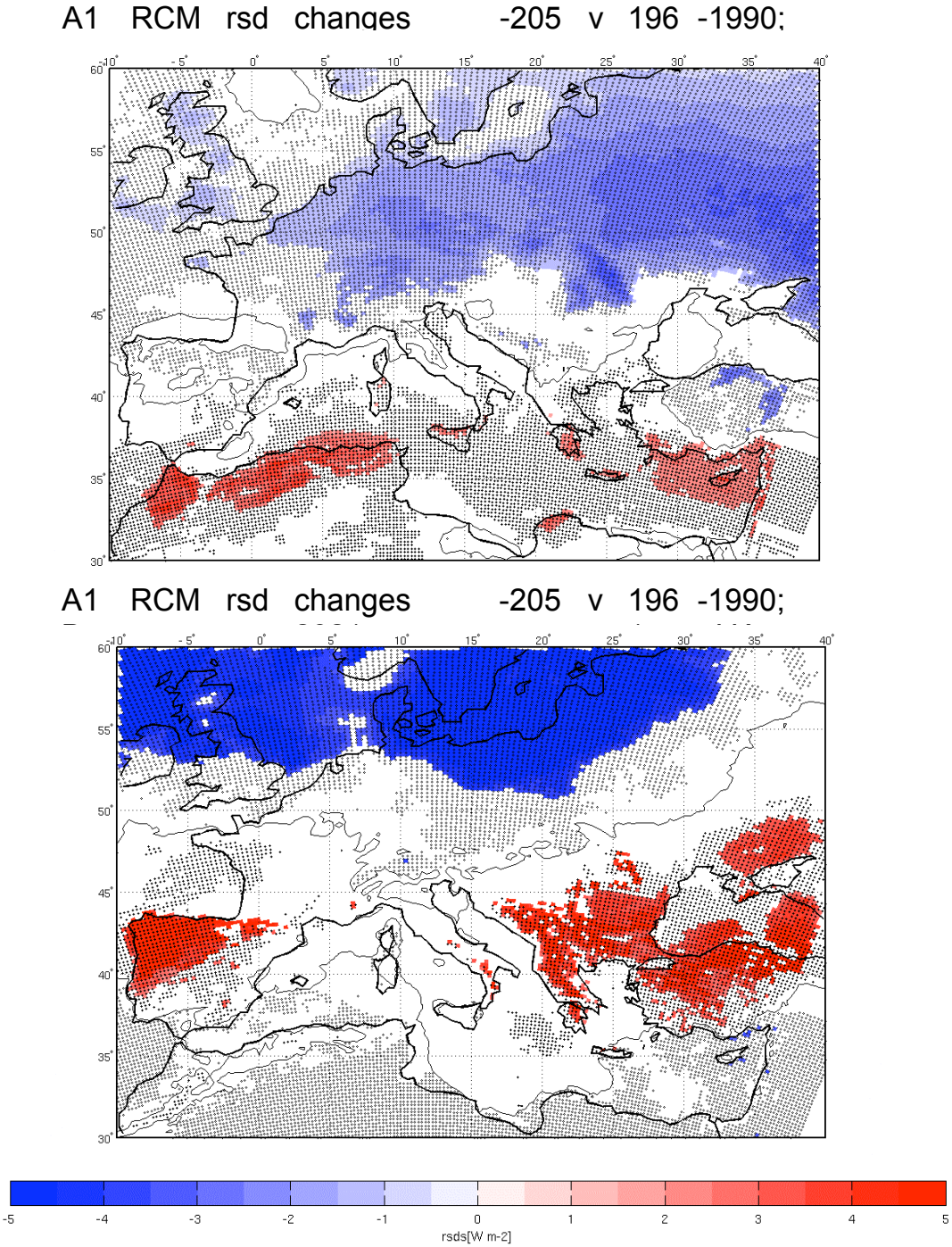

Figure 4.4 :*Mean changes in surface shortwave solar radiation (rsds) projected by A1B scenario RCMs ENSEMBLES simulations. Colours represent the average long term change in rsds projected for 2021-2050 with respect to 1961-1990. Model data are produced at an horizontal resolution of 25Km . Hatched areas represent areas where more than 66% of the model agree in the sign of the long term change. We report only changes statistically significant at the 90% confidence level (t-*

test). The solid lines are for zero contour.

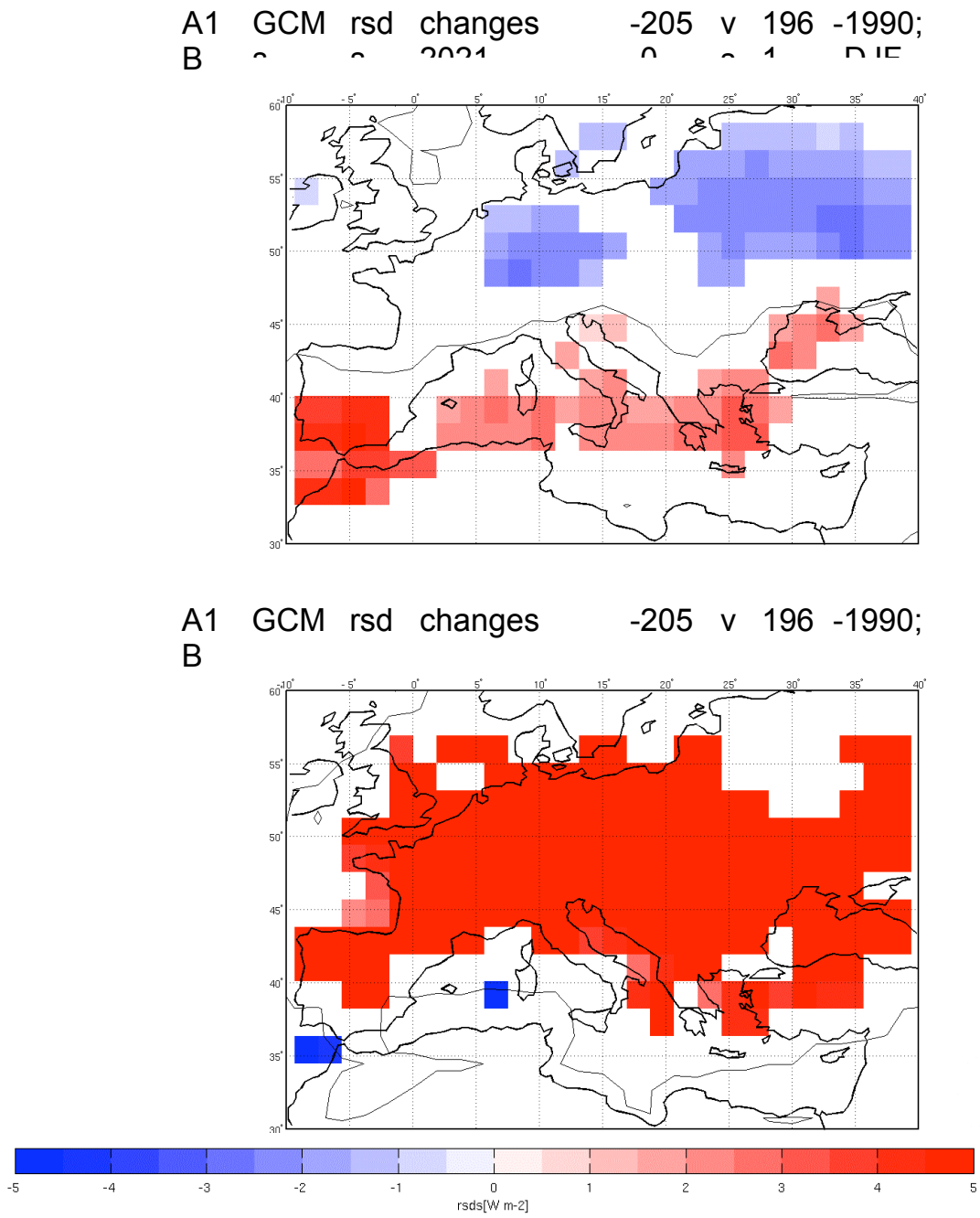

Figure 4.5: *Mean changes in surface shortwave solar radiation (rsds) projected by A1B GCMs scenario simulations driving the RCMs ENSEMBLES runs (see table1). Colours represent the average long term change in rsds projected for 2021-2050 with respect to 1961-1990. We report only changes statistically significant at the 90% confidence level (t-test). The solid lines are for zero contour.*

From the previous analysis, Spain stands out as one of areas most sensibly affected by the 21st century projected changes in solar radiation (both in winter and summer seasons). Here we focus on one specific site, Andalucia (Fig. 4.6). At this site, the solar radiation increases significantly in the future but the uncertainty between models can be strong and the interannual variability can be high.

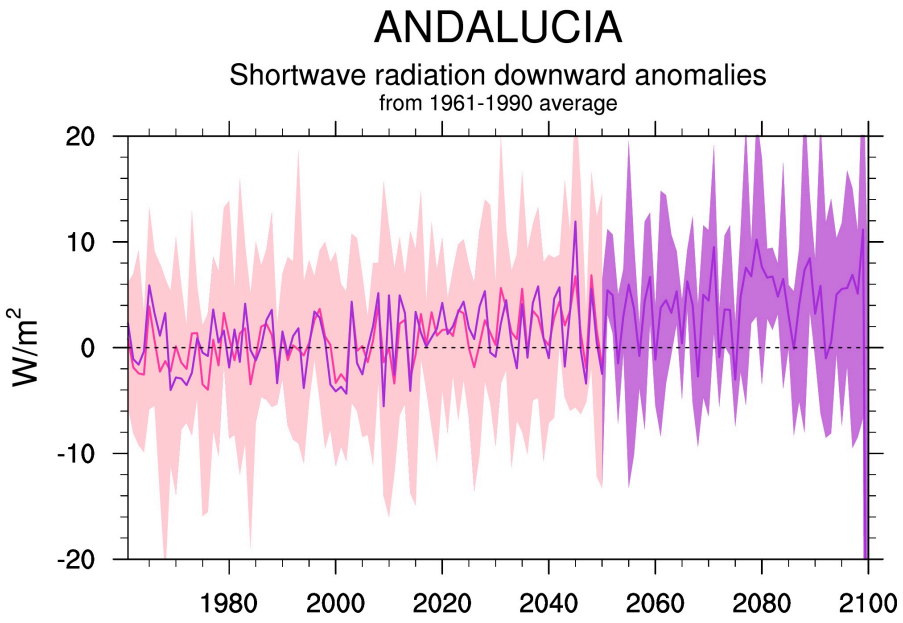

***Figure 4.6**: Change in solar radiation in Andalucia (20 models cover the period up to 2050 and 16 up to 2100).*

5. Forest fire

5.1 Future fire risk projections for the Mediterranean region

Forest fire risk was assessed using the Canadian Fire Weather Index (FWI). FWI is a daily meteorological-based index used worldwide to estimate fire danger in a generalized fuel type. Although it has been developed for Canadian forests, several studies have shown its suitability for the Mediterranean basin (e.g. Moriondo et al. 2006). The FWI System provides numerical ratings of relative fire potential based solely on weather observations. FWI components depend on daily noon

measurements of dry-bulb temperature, air relative humidity, 10m wind speed and 24 h accumulated precipitation and are described in detail in van Wagner (1987). FWI consists of 6 standard components each measuring a different aspect of fire danger. The first three are fuel moisture codes that follow daily changes in the moisture contents of three classes of forest fuel with different drying rates. The remaining components are fire behaviour indices representing the rate of spread, fuel weight consumed and fire intensity.

Daily output data from three regional climate models (RCMs) developed at KNMI (Netherlands), ETHZ (Switzerland) and MPI (Germany) within the framework of the EU ENSEMBLES project have been used [www.ensembles-eu.org]. All models have a horizontal resolution of 25 km × 25 km and use the A1B greenhouse gases emissions scenario (Nakicenovic et al., 2000). Present day simulations cover the period 1961-1990 and are used here as reference for comparison with future projections for the periods 2021-2050 (near future) and 2071-2100 (distant future).

As found in previous studies (Hanson and Palutikof, 2005), fire risk is low for FWI<15, and increases more rapidly with FWI>15. In this study a threshold of FWI>15 was selected as a measure of fire risk in the area of interest and FWI>30 was selected as a measure of elevated fire risk.

For the Mediterranean region, the ensemble mean of the models was calculated and the maps produced illustrate the number of days with fire risk (FWI>15) and elevated (FWI>30) fire risk for the control period (1961-1990) as well as the changes in the number of days with fire risk and elevated fire risk between the reference and the two future periods (Fig. 5.1).

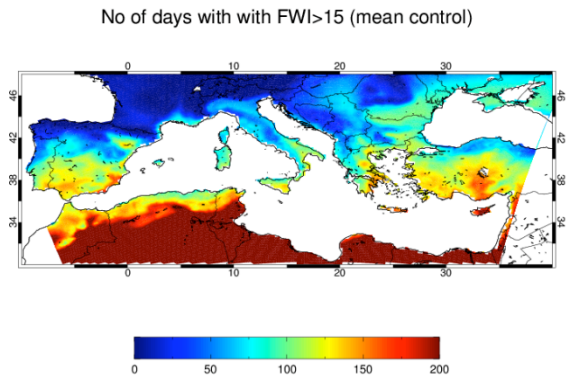

(a)

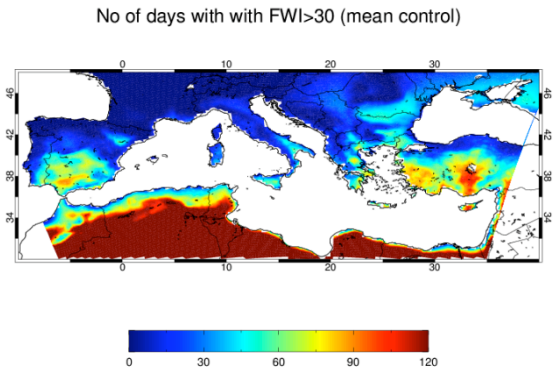

(b)

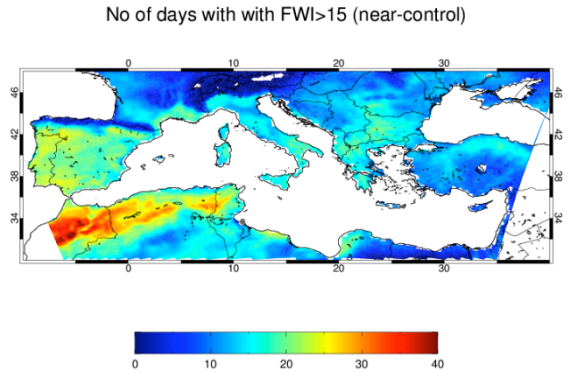

(c)

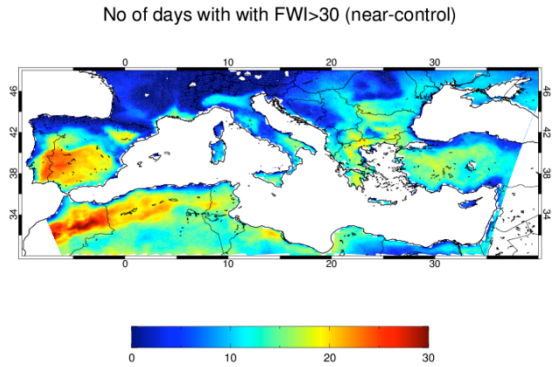

(d)

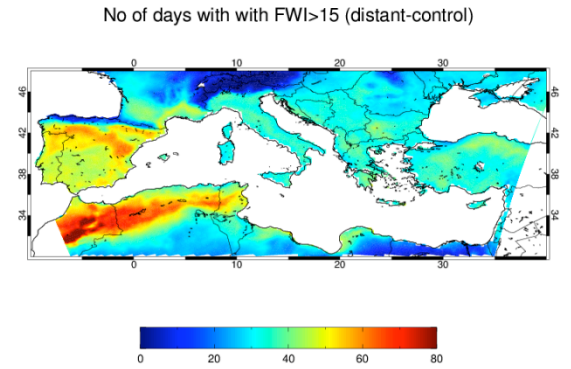

(e)

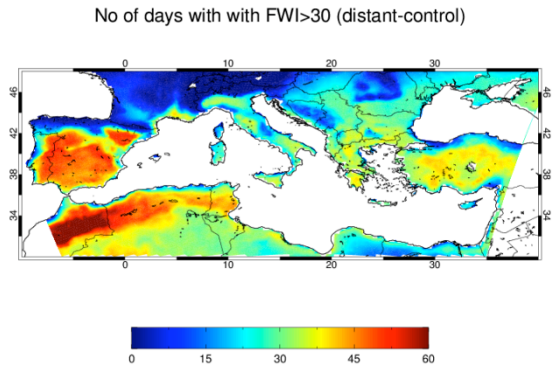

(f)

***Figure 5.1**: Ensemble mean of three ENSEMBLES RCMs for the control period 1961-1990 for the number of days with fire risk FWI>15 (a) and elevated fire risk FWI>30 (b), the differences*

between the near future 2021-2050 and the control period in the number of days with fire risk FWI>15 (c) and elevated fire risk FWI>30 (d) and the differences between the distant future 2071-2100 and the control period in the number of days with fire risk FWI>15 (e) and elevated fire risk FWI>30 (f).

As shown in Fig. 5.1, the days with fire risk are expected to increase in the entire domain by up to 1 month for the near future. Regarding elevated fire risk, an increase of one month per year is expected in the southern part of the Iberian Peninsula and Northwestern Africa. In Eastern continental Greece, Italy and Sicilia an increase of up to 20 more days with elevated fire risk is estimated.
The increase in the days of fire risk is even greater for the distant future and exceeds two months in the western part of the domain (Iberian peninsula, Northwestern Africa). Regarding elevated fire risk, the period of elevated fire risk lengthens substantially, reaching 60 more days per year for the Iberian Peninsula, and Northwestern Africa. Furthermore, substantial increases of approximately 30 days or more will be evident in Greece, Italy and Sicilia. Finally, by the end of the century, an increase of up to 40 more days per year with elevated fire risk is expected for the south of France.

5.2 Evaluation and evolution of fire risk: Greece case study

To study fire risk for the case study of Greece, two regions of interest were chosen, the national conservation park of Sounio located in the south tip of the Attica peninsula and the archeological site of Olympia in the western part of Peloponnese (Figure 5.2). Both areas are prone to fire events therefore determination of fire risk in these areas is of added significance.

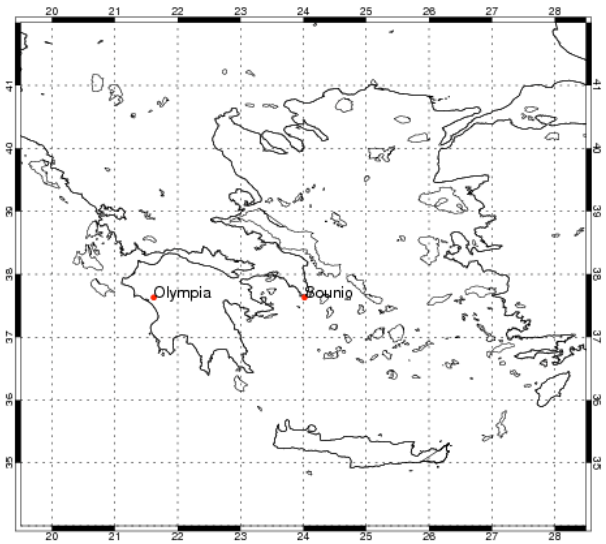

Figure 5.2 *Map of Greece with the location of the two selected regions.*

Daily meteorological data for these two regions covering the period 1961-1990 were obtained from the Hellenic National Meteorological Service. Daily values of FWI were calculated these

observations and subsequently were compared with the index values of the ensemble mean of the models for the nearest grid point.
Figure 5.3 depicts mean monthly values of FWI of the ensemble mean for the reference (1961-1990) and the two future periods (2021-2050 and 2071-2100) as well as mean monthly FWI values calculated from the observational data set for the reference period. The calculation of the index was performed only for the fire season, which covers the months from May to October. As far as the reference period is concerned, the models slightly underestimate the index during May and June and overestimate it during the other months.
Moreover, throughout the fire season, the models are consistent and indicate the highest FWI values during July and August, when indeed most fire events occur. The same pattern occurs for the future periods, but the values of risk are substantially increased and reach 42 in Sounio and 35 in Olympia in July and August.

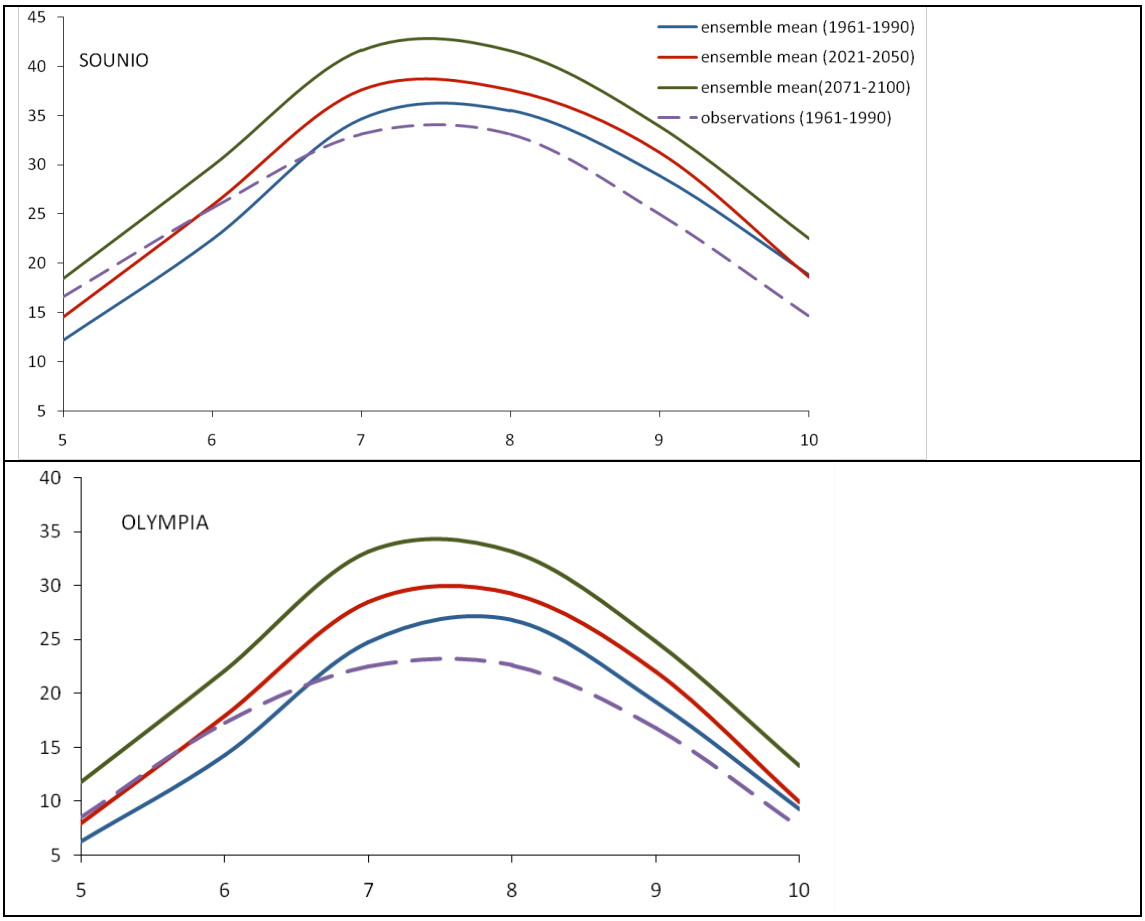

***Figure 5.3**: Mean monthly FWI values of the ensemble mean of the models for the period 1961-1990(blue line), 2021-2050 (red line), 2071-2100 (green line) and of the observations for the period 1961-1990 (purple line).*

Figure 5.4 shows mean summer values of FWI for the ensemble mean of the models for Sounio and Olympia, for the whole examined period i.e. from 1961 to 2100. A positive trend is observed for

both regions with Sounio depicting higher summer reaching or exceeding 40 near the end of the century.

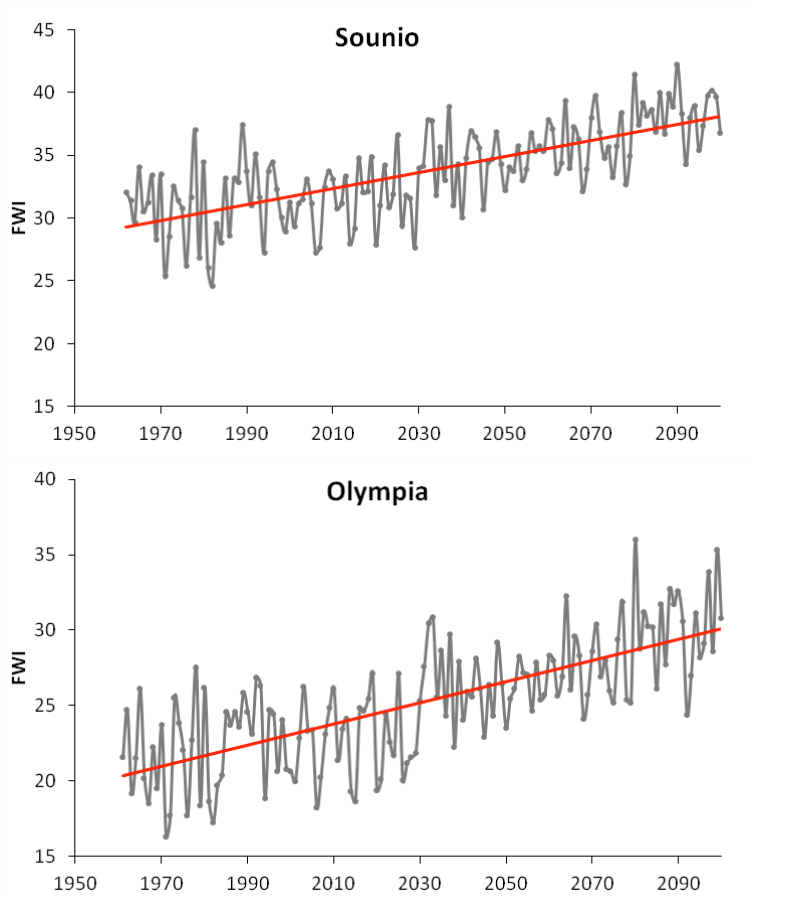

***Figure 5.4**: Mean summer FWI values of the ensemble mean of the models covering the period 1961-2100.*

6. Tourism Climate Index (TCI)

Within the CLIM-RUN project, the Tourism Climate Index (TCI) was identified as a reliable indicator for tourism quality in the Mediterranean region. The TCI was first introduced by Mieczkowski (1985) and is based on maximum temperature, humidity, wind, and sunshine duration. Previous studies showed that regional climate models (RCMs) provide a reasonable representation of the present climate in a region with complex orography and in coastal areas. Here, we try to calculate the TCI using the simulations from the EU-FP6 ENSEMBLES Project.

Institute	Scenario	Driving GCM	Model	Resolution	End year
CNRM	AIB	ARPEGE	Aladin	25kms	2100
KNMI	AIB	ECHAM5-3	RACMO	25kms	2100
OURANOS	AIB	CGXM3	CRCM	25kms	2100
SMHI	AIB	BCM	RCA	25kms	2100
	AIB	ECHAM-r3	RCA	25kms	2100
	AIB	HadCMQ3	RCA	25kms	2100
MPI	AIB	ECHAM-r3	REMO	25kms	2100
METNO	AIB	BCM	HIRHAM	25kms	2050
	AIB	HadCM3QO	HIRHAM	25kms	2050
C4I	AIB	HadCM3Q16	RCA3	25kms	2100
UCLM	AIB	HadCM3Q0	PROMES	25kms	2050
ETHZ	AIB	HadCM3Q0	CLM	25kms	2099
HC	AIB	HadCM3Q0	HadRM3Q0	25kms	2100
	AIB	HadCM3Q0	HadRM3Q3 (low sensitivity)	25kms	2100
	AIB	HadCM3Q16	HadRM3Q16 (high sensitivity)	25kms	2100
DMI	AIB	ARPEGE	HIRHAM	25kms	2100
	AIB	ECHAM5-r3	DMI-HIRHAM5	25kms	2099
	AIB	BCM	DMI-HIRHAM5	25kms	2099
ICTP	AIB	ECHAM5-r3	RegCM	25kms	2100
VMGO	AIB	HadCM3Q0	RRCM	25kms	2050

Table 6.1*: List of the models available from the ENSEMBLE project. Only the shaded ones have been used in the present analysis, as they provide all the variables needed to calculate the TCI.*

The TCI diagnosed for the present climate (1971-2000; Fig. 6.1) period, in summer, shows that the index is higher over the northern part of the Mediterranean region. Northern Europe and Sahara regions show the lowest TCI values. While there is a reasonable model-to-model agreement in the TCI spatial distribution, large discrepancies are found in the absolute values of the TCI. In one particular model, the TCI does never exceed 70 in the summer season.
Based on the TCI value, the number of days greater than 70 can be calculated over the three summer months (Fig. 6.2). The ensemble mean has about 50 comfortable days during the summer over the southern Europe. One model has no value higher than 70 during the entire summer season.

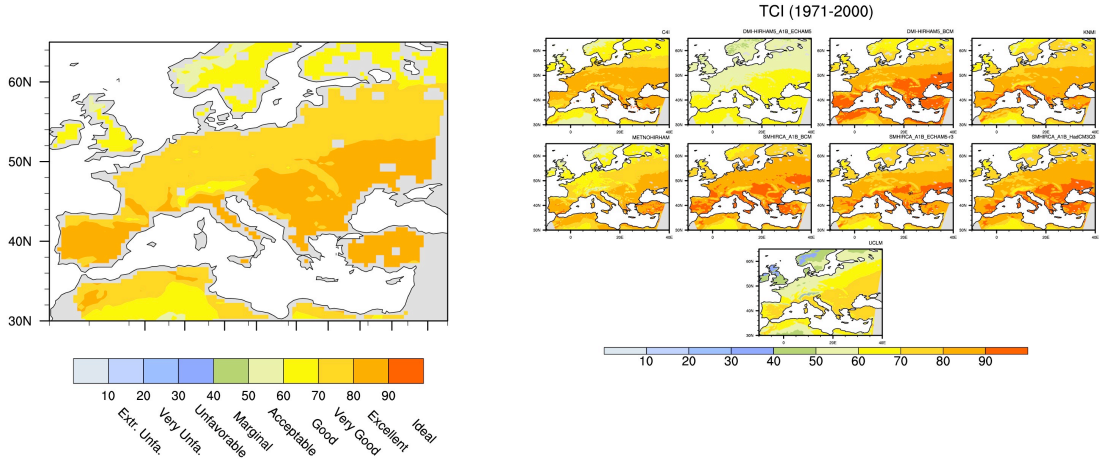

***Figure 6.1**: TCI calculated for the ENSEMBLES mean (left) and for the nine different models over the period 1971-2000 during the summer season.*

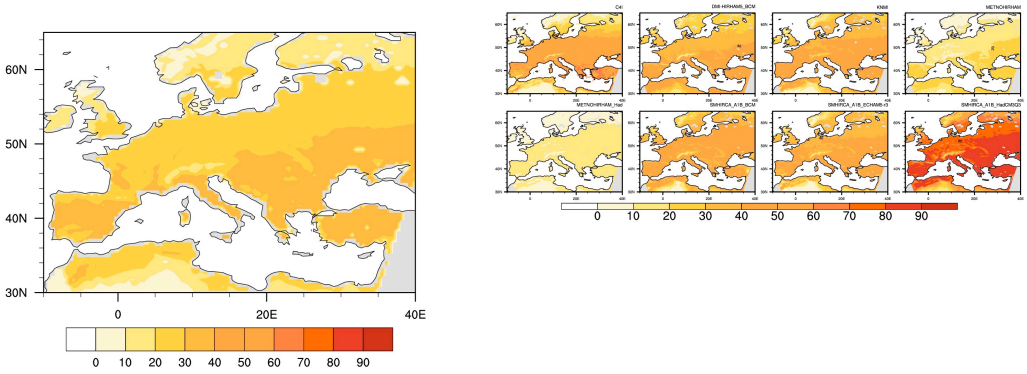

***Figure 6.2**: Number of days where the TCI is greater than 70 over the summer season for the period 1971-2000. Left (ensembles mean), right (individuals models). (One model has no TCI greater than 70 during the summer months).*

Under climate change, the temperature is expected to increase and also precipitation humidity, wind and so on are expected to change. In the near future (2021-2050), the TCI is increasing on average north of 45°N and is decreasing further south (Fig. 6.3). The change in the TCI (Fig. 6.4) is weak and does not show any gain in the number of days greater than 70 north of 45°N. On the other side,

the number of days greater than 70 is decreasing south of 45°N with the strongest decrease in northern Africa.

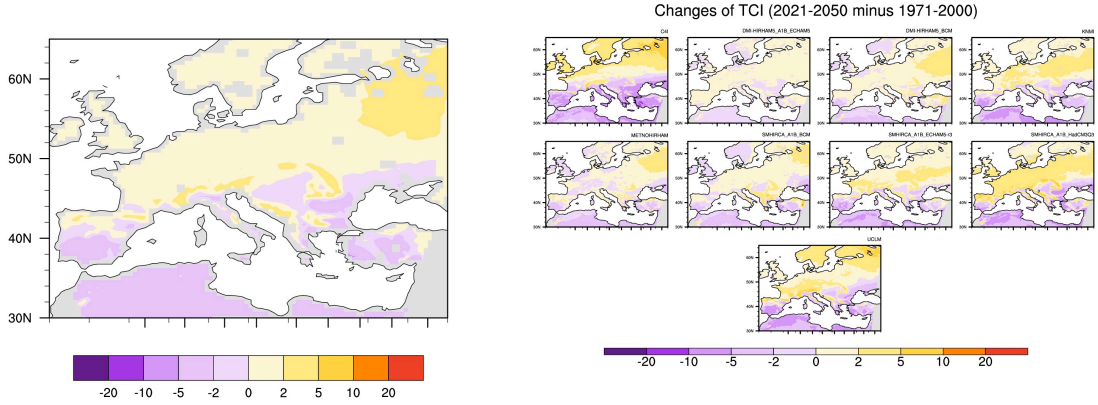

***Figure 6.3**: Change of the TCI for the period 2021-2050 compared to the 1971-2000 period. On the left: ensemble mean, right: individual model.*

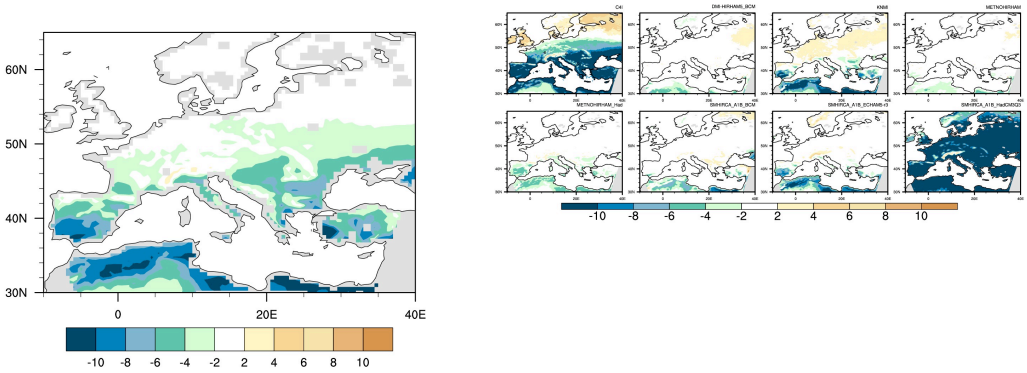

***Figure 6.4**: Change in the number of days with a TCI greater than 70 over the summer season for the period 2021-2050 compared to the 1971-2000 period. Left (ensembles mean), right (individuals models).*

7. Surface temperature

7.1 Future evolution of sea surface temperature in coastal regions.

Under climate change, bathing conditions are expected to change. Those changes can have strong impacts on the practice of the surrounding sea and the use of the coastal zone. Consequently tourism stakeholders expressed the needs for climate information about the possible change of the sea surface temperature in the surrounding sea.
The evolution of the sea surface temperature (SST) is analysed at four different geographical locations: Venice lagoon, Croatian coastal region, Gulf of Gabes in Tunisia and surrounding sea around Cyprus island. They are defined by the following coordinates:

- Venice: 11.46-13.5°E/44.47-45.5°N
- Croatia: 13.3-15°E/44.3-45.7°N
- Tunisia (Gulf of Gabes): 7.5-11.6°E/30.22-37.35°N
- Cyprus island: geographical island

The SST needs to be represented by a high spatial resolution of the Mediterranean sea accounting for the complex bathymetry and morphology of the Mediterranean basin. Coupled atmosphere-ocean regional climate change simulations over the Mediterranean sea have been carried out within the CIRCE FP7 Project. Those simulations illustrate the possible climate change over the period 1950 to 2050 in the future following the A1B emissions scenarios . Those simulations were carried out by five different coupled atmosphere-ocean regional climate models (AORCM) coming from the following institutes: ENEA, MPI, INGV, LMD and CNRM. Those models are high resolution coupled atmosphere-ocean regional climate models (10 km horizontal resolution in the ocean).
Here, we present the change in the sea surface temperature (SST) over the period 1950-2050 compared to the reference period: 1961-1990 at the afore-mentioned four different sites (Fig. 7.1).
The SSTs are increasing in the future at all sites. The increase is stronger at the end of the 21st century. By the end of the century, the increase is on average between 1.8 to 2°C. The warming is stronger in North Adriatic and Croatia regions.
We are aware that the products delivered here may underestimate the uncertainty due to the use of only 5 AORCMs and 1 scenario. These simulations were the first realized with AORCMs over the Mediterranean sea. However we think that a new generation of high resolution AORCMs is required to better assess the evolution of SST accounting for the complex bathymetry of the Mediterranean sea. The Med-CORDEX project will provide a larger ensemble of high resolution regional climate simulations over the 21st century under different emissions scenarios, focusing on the Mediterranean region. This set of simulations will provide a more accurate estimate of the uncertainties associated with the projected climate change. Futhermore, if observations timeseries were collected at the four reference sites, statistical corrections could be applied. This could also give us the possibility to define a bathing index.

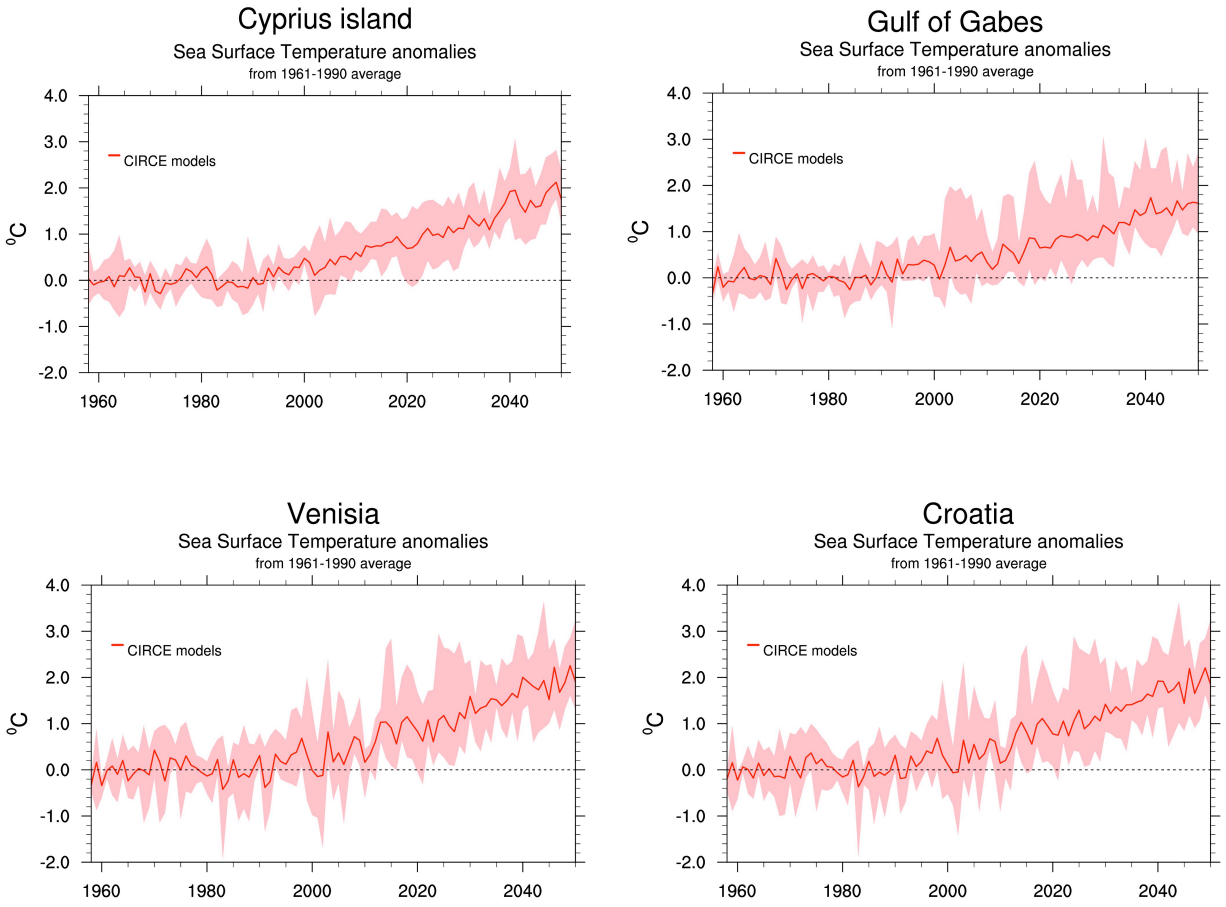

***Figure 7.1**: Evolution of the yearly sst at four different sites over the 21st century compared to the reference period 1961-1990. In shaded pink, the minimum/maximum change of the SST and in red the ensemble mean of the 5 simulations.*

7.2 Future evolution of summer temperature in Savoie.

Under climate change, the evolution of the summer temperatures in Savoie at different altitude level have an influence on the tourism activities. Those changes have strong impacts on the practice of outdoors activities in mountainous region especially at the highest level.
Simulations of climate change over mountainous regions have been carried out within the ANR/SCAMPEI project (http://www.cnrm.meteo.fr/scampei/presentation_scampei/index.php). The simulations were carried out by the LMD, LGGE and CNRM at Météo France using high resolution

regional climate models at a 12 km horizontal resolution. A statistical analysis is applied to take into account the complex orography in mountainous regions. The simulations have been run over 3 different periods: the present period (1961-1990), the near future (2021-2050) and the far future (2071-2100).
Here, we present the change in maximum and minimum temperatures during the summer season in Savoie for different altitude ranges. The longitude-latitude range used to define the Savoie region is [5.87-7.07°E; 45.17-46.5°N].
At all levels, the temperature is increasing. At the end of the century this increase is up to 6°C.

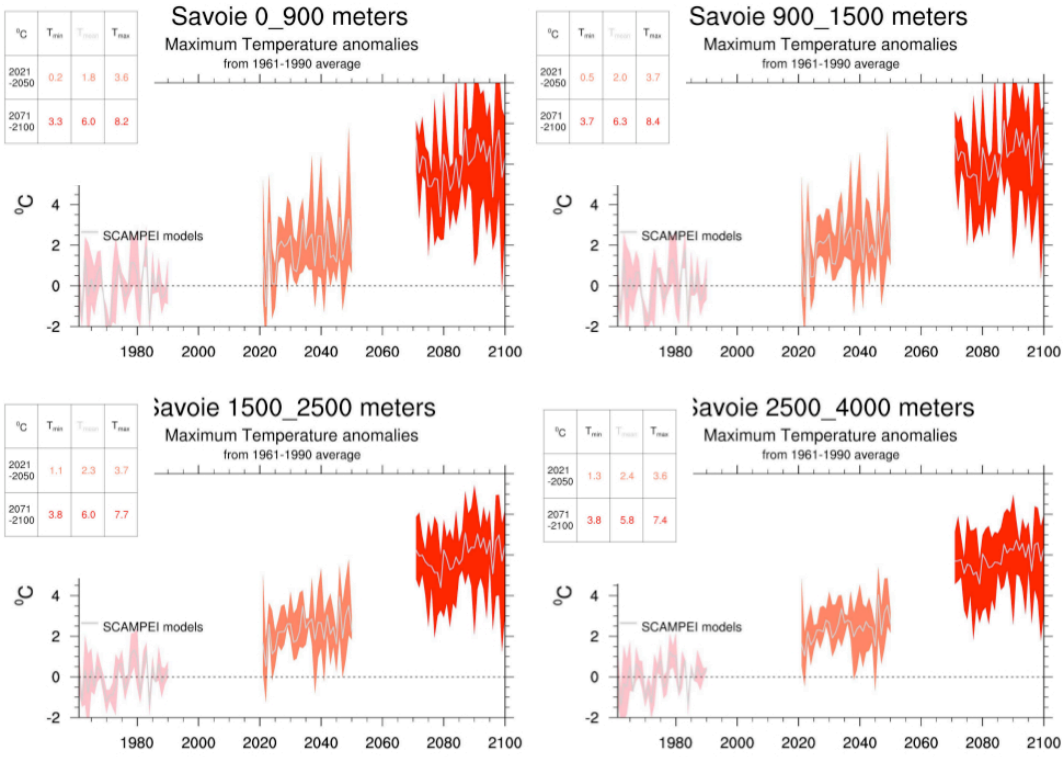

***Figure 7.2**: Evolution of the maximum temperatures in Savoie for the different altitudes ranges compare to the reference period 1961-1990.*

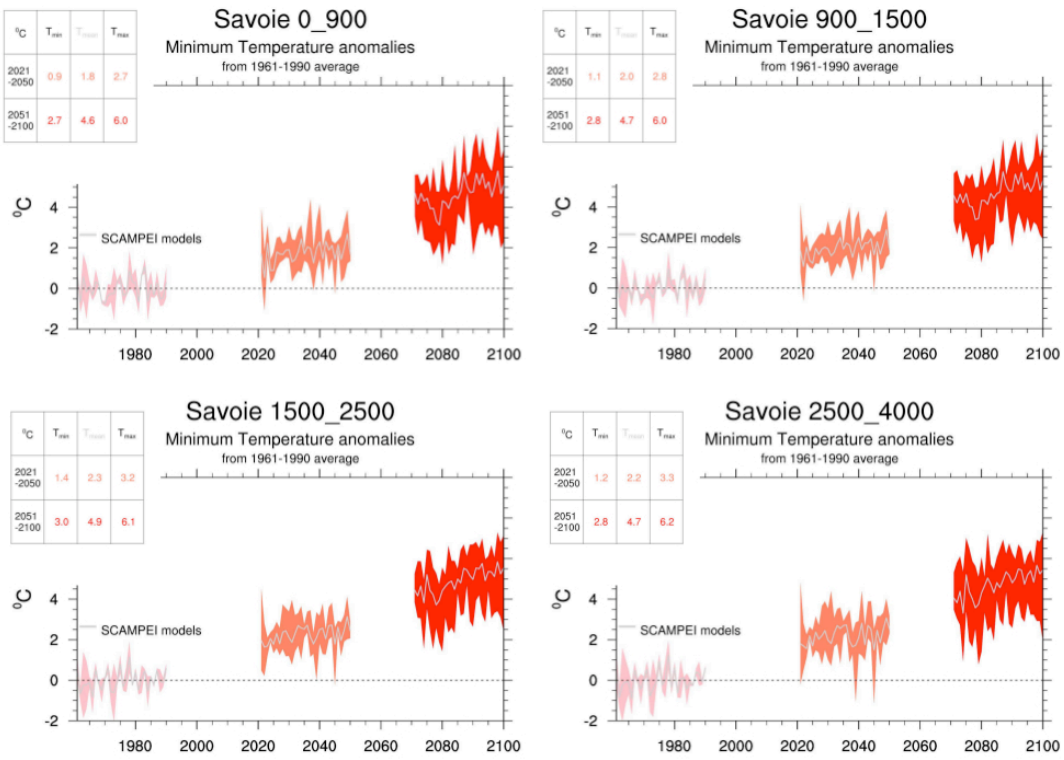

***Figure 7.3**: Evolution of the minimum temperatures in Savoie for the different altitudes ranges compare to the reference period 1961-1990.*

References

References (Intro)

Christensen, J.H., and Co-authors, 2007: Regional Climate Projections. In: *Climate Change 2007: The Physical Science Basis. Contribution of Working Group I to the Fourth Assessment Report of the Intergovernmental Panel on Climate Change* [Solomon, S., D. Qin, M. Manning, Z. Chen, M. Marquis, K.B. Averyt, M. Tignor and H.L. Miller (eds.)]. Cambridge University Press, Cambridge, United Kingdom and New York, NY, USA.

Mediterranean Climate Variability, 2006: Lionello, P., P. Malanotte, and R. Boscolo (eds.),. Elsevier B.V.

The climate of the Mediterranean Region: from the past to the future, 2012: Lionello, P. Editor, Elsevier.

Regional Assessment of the Climate Change in the Mediterranean: Air, Sea and Precipitation and Water, A. Navarra and L. Tubiana, Eds., Advances in Global Change Research, Vol. 50, Springer Verlag, 125.

References (Sea-level)

Gualdi, S., and Coauthors, 2012: Future climate projections. Regional Assessment of the Climate Change in the Mediterranean: Air, Sea and Precipitation and Water, A. Navarra and L. Tubiana, Eds., Advances in Global Change Research, Vol. 50, Springer Verlag, 125.

Gualdi S., and Coauthors, 2013: The CIRCE simulations: a new set of regional climate change projections performed with a realistic representation of the Mediterranean Sea., *Bulletin of American Meteorological Society*, 94, 65-81, DOI: http://dx.doi.org/10.1175/BAMS-D-11-00136.1.

Jordà, G., and D. Gomis, 2013: On the interpretation of the steric and mass components of sea level variability: The case of the Mediterranean basin, J. Geophys. Res.: Oceans, 118, doi:10.1002/jgrc.20060.

Katsman, C. A., W. Hazeleger, S. S. Drijfhout, G. J. van Oldenborgh, and G. Burgers, 2008: Climate scenarios of sea level rise for the northeast Atlantic ocean: a study including the effects of ocean dynamics and gravity changes induced by ice melt, Clim. Change, 91, 351–374, doi:10.1007/s10584-008-9442-9.

Marcos, M., and M. N. Tsimplis, 2008: Comparison of results of AOGCMs in the Mediterranean Sea during the 21st century. J. Geophys. Res., 113, C12028, doi:10.1029/2008JC004820.

Okumura, Y. M., C. Deser, A. Hu, A. Timmermann, and S.-P. Xie, 2009: North Pacific Climate Response to Freshwater Forcing in the Subarctic North Atlantic: Oceanic and Atmospheric Pathways, J. Climate, 22, 1424–1445, doi:10.1175/ 2008JCLI2511.1.

Somot, S., F. Sevault, M. Déqué, and M. Crépon, 2008: 21st century climate change scenario for the Mediterranean using a coupled atmosphere-ocean regional climate model. Global Planet. Change, 63, 112–126.

Tsimplis, M., M. Marcos, and S. Somot, 2008: 21st century Mediterranean sea level rise: Steric and atmospheric pressure contributions from a regional model. Global Planet. Change, 63, 105–111, doi:10.1016/j.gloplacha.2007.09.006.

References (Wind)

Artale et al. (2009). An atmosphere-ocean regional climate model for the Mediterranean area: assessment of a present climate simulation. Clim. Dyn. doi:10.1007/s00382-009-0691-8

Christensen, J. H., M. Rummukainen, G. Lenderink, (2009). Formulation of very-high-resolution regional climate model ensembles for Europe. In: van der Linden P., and J.F.B. Mitchell (eds.). *ENSEMBLES: Climate Change and its Impacts: Summary of research and results from the ENSEMBLES project*. Met Office Hadley Centre, FitzRoy Road, Exeter EX1 3PB, UK. 160pp

Simmons AJ, Gibson JK (2000) The ERA-40 Project Plan, ERA-40 project report series no. 1 ECMWF, p 62.

Ruti, P. M., S. Marullo, F. D'Ortensio and M Tremant, (2008): Comparison of analyzed and measured wind speeds in the perspective of oceanic simulations over the Mediterranean basin: analyses, QuikSCAT and buoy data. Journal of Marine Systems, 70, 33-48 doi:10.1016/j.jmarsys.2007.02.02.

Feser et al., Regional climate models add value to global model data". Bull. Of the American Meteorological Society 92 (2011): 1181-1192.

Winterfeldt J. and R. Weisse, 2009: Assessment of value added for surface marine wind speed obtained from two regional climate models. Mon. Wea. Rev., 137:2955-2965. DOI:10.1175/2009MWR2704.1.

Winterfeldt J., Geyer, B. and Weisse R., 2011: Using QuikSCAT in the added value assessment of dynamically downscaled wind speed. In. J. Climatol., 31: 1028-1039. Doi:10.1002/joc.2105

References (Solar radiation)

Boé, J., Terray L., Cassou C., Najac J., 2009: Uncertainties in European summer precipitation changes: role of large scale circulation. Volume 33, Issue 2-3, pp 265-276

Déqué, M., Somot, S., Sanchez-Gomez, E., Goodess, C. M., Jacob, D., Lenderink, G., & Christensen, O. B. (2012). The spread amongst ENSEMBLES regional scenarios: regional climate models, driving general circulation models and interannual variability. Climate dynamics, 38(5-6), 951-964

Fu, Qiang, K. N. Liou, M. C. Cribb, T. P. Charlock, A. Grossman, 1997: Multiple Scattering Parameterization in Thermal Infrared Radiative Transfer.J. Atmos. Sci., 54, 2799–2812.

Gupta, Shashi K., Wayne L. Darnell, and Anne C. Wilber, 1992: A Parameterization for Longwave Surface Radiation from Satellite Data: Recent Improvements. J. Appl. Meteorol., 31,1361-1367, doi:10.1175/1520-0450(1992)031.

Gupta, Shashi K., David P. Kratz, Paul W. Stackhouse, Jr., and Anne C. Wilber, 2001: The Langley Parameterized Shortwave Algorithm (LPSA) for Surface Radiation Budget Studies (Version 1.0). NASA Tech Reports, NASA/TP-2001-211272, 31pp.

Konzelmann, T., D. R. Cahoon, and C. H. Whitlock 1996: Impact of biomass burning in equatorial Africa on the downward surface shortwave irradiance: Observations versus calculations. J. Geophys. Res., 101, 22 833-22 844.

Pinker, R. T., and I. Laszlo, 1992: Modeling of surface solar irradiance for satellite applications on a global scale. J. Appl. Meteor., 31, 194–211.

References (Fire)

Hanson CE, Palutikof JP (2005) Final report of Modelling the Impacts of Climate extremes (MICE) Project. Project number: EVK2-CT-2001-00118.

Moriondo, M, Good P, Durao R, Bindi M, Giannakopoulos C, Corte-Real J (2006) Potential impact of climate change on fire risk in the Mediterranean area. Clim Res 31:85–95. doi:10.3354/cr031085.

Nakicenovic N, Alcamo J, Davis G, et al. (2000) Special Report on Emission Scenarios, Working Group III of the Intergovernmental Panel on Climate Change (IPCC). Cambridge University Press, Cambridge, 595 pp.

Van Wagner CE (1987) Development and structure of a Canadian forest fire weather index system, Forestry Technical Report 35. Canadian Forestry Service, Ottawa.

References (TCI)

References (Surface Temperature)